

Supplementary Information

Hypolectronic Titanaboranes: Icosahedral and Tetracapped Tetrahedral Clusters Comprising Bridging Hydrides

Subhash Bairagi, Debipada Chatterjee,[‡] Soumen Giri[‡] and Sundargopal Ghosh*

Department of Chemistry, Indian Institute of Technology Madras, Chennai 600036, India, E-mail: sghosh@iitm.ac.in

[‡]These authors contributed equally to this work.

Table of contents

I	Experimental Details	
Scheme S1	Synthesis of 1 .	S5
Scheme S2	Synthesis of 2 .	S6
Scheme S3	Synthesis of 3a and 3b .	S6
I.1	UV-visible Studies	S7
I.2	Supplementary Data	
Figure S1	Molecular structure and labelling diagram of 1 .	S8
Figure S2	Icosahedron core [Ti ₃ B ₉] of 1 .	S8
Figure S3	Molecular structure and labelling diagram of 2 .	S9
Figure S4	Tetracapped tetrahedron [Ti ₃ B ₃ Te ₂] core of 2 .	S9
Figure S5	Molecular structure and labelling diagram of 3b .	S10
Figure S6	[Ti ₂ B ₅] core of 3b .	S10
I.3	Spectroscopic Details	
Figure S7	ESI-MS spectrum of 1 .	S11
Figure S8	¹¹ B{ ¹ H} NMR spectrum of 1 .	S11
Figure S9	¹¹ B NMR spectrum of 1 .	S12
Figure S10	¹ H NMR spectrum of 1 .	S12
Figure S11	¹³ C{ ¹ H} NMR spectrum of 1 .	S13
Figure S12	IR spectrum of 1 .	S13
Figure S13	ESI-MS spectrum of 2 .	S14
Figure S14	¹¹ B{ ¹ H} NMR spectrum of 2 .	S14
Figure S15	¹ H NMR spectrum of 2 .	S15
Figure S16	¹ H{ ¹¹ B} NMR spectrum of 2 .	S15
Figure S17	Stacked ¹ H (bottom) and ¹ H{ ¹¹ B} NMR (top) spectra of 2 .	S15
Figure S18	¹ H- ¹¹ B HSQC NMR spectrum of 2 .	S16
Figure S19	IR spectrum of 2 .	S16
Figure S20	ESI-MS spectrum of 3a .	S17
Figure S21	¹¹ B{ ¹ H} NMR spectrum of 3a .	S17
Figure S22	¹¹ B NMR spectrum of 3a .	S18
Figure S23	¹ H NMR spectrum of 3a .	S18
Figure S24	¹ H{ ¹¹ B} NMR spectrum of 3a .	S19
Figure S25	Stacked ¹ H (bottom) and ¹ H{ ¹¹ B} NMR (top) spectra of 3a .	S19
Figure S26	¹³ C{ ¹ H} NMR spectrum of 3a .	S19
Figure S27	⁷⁷ Se NMR spectrum of 3a .	S20
Figure S28	IR spectrum of 3a .	S20
Figure S29	ESI-MS spectrum of 3b .	S21

Figure S30	$^{11}\text{B}\{^1\text{H}\}$ NMR spectrum of 3b .	S21
Figure S31	^{11}B NMR spectrum of 3b .	S22
Figure S32	^1H NMR spectrum of 3b .	S22
Figure S33	$^1\text{H}\{^{11}\text{B}\}$ NMR spectrum of 3b .	S23
Figure S34	Stacked ^1H (bottom) and $^1\text{H}\{^{11}\text{B}\}$ NMR (top) spectra of 3b .	S23
Figure S35	$^{13}\text{C}\{^1\text{H}\}$ NMR spectrum of 3b .	S23
Figure S36	^{77}Se NMR spectrum of 3b .	S24
Figure S37	IR spectrum of 3b .	S24
Figure S38	Combined UV-vis spectra of 1 , 2 , 3a , and 3b in CH_2Cl_2 .	S25
I.4	X-ray Analysis Details	S26
II	Computational Details	S26
Table S1	Selected geometrical parameters and Wiberg bond indices (WBI) of 1 , 2 , 3a , and 3b .	S27
Table S2	Selected experimental and Calculated bond angles of 1 , 2 , 3a , and 3b .	S28
Table S3	Calculated natural charges (q) and natural valence population (Pop) of 1 , 2 , 3a , and 3b .	S28
Table S4	Calculated HOMO–LUMO energy gap of 1 , 2 , 3a , and 3b .	S29
Table S5	Calculated ^{11}B chemical shifts for complexes 1 , 2 , 3a , and 3b .	S29
Figure S39	Selected molecular orbitals of 1 .	S30
Figure S40	Selected NBO interactions of 1 .	S30
Figure S41	Contour-line diagram of the Laplacian of the electron density of 1 in selected planes.	S31
Figure S42	Selected molecular orbitals of 2 .	S31
Figure S43	Selected NBO interactions of 2 .	S32
Figure S44	Contour-line diagram of the Laplacian of the electron density of 2 in selected planes.	S32
Figure S45	Selected molecular orbitals of 3a .	S33
Figure S46	Selected NBO interactions of 3a .	S33
Figure S47	Contour-line diagram of the Laplacian of the electron density of 3a in selected planes.	S34
Figure S48	(a) Selected NBO interaction of 3b . (b) Contour-line diagram of the Laplacian of the electron density of 3b along B2-C1-C2 plane.	S34
Figure S49	Absorption spectrum of 1 computed at TD-DFT-B3LYP/Def2-SVP level of theory.	S35
Table S6	TD-DFT calculated energies (excitation energy (eV), λ_{calc} (nm)), oscillator strength (f), and main composition of the first UV–vis electronic excitations for 1 . Experimental absorption wavelengths (λ_{exp} , nm) of 1 are given for comparison.	S35
Figure S50	Selected molecular orbitals of 1 related to most intense electronic transitions.	S36
Figure S51	Absorption spectrum of 2 computed at TD-DFT-B3LYP/Def2-SVP level of theory.	S36
Table S7	TD-DFT calculated energies (excitation energy (eV), λ_{calc} (nm)), oscillator strength (f), and main composition of the first UV–vis electronic excitations for 2 . Experimental absorption wavelengths (λ_{exp} , nm) of 2 are given for comparison.	S37
Figure S52	Selected molecular orbitals of 2 related to most intense electronic transitions.	S38
Figure S53	Absorption spectrum of 3a computed at TD-DFT-B3LYP/Def2-SVP level of theory.	S38

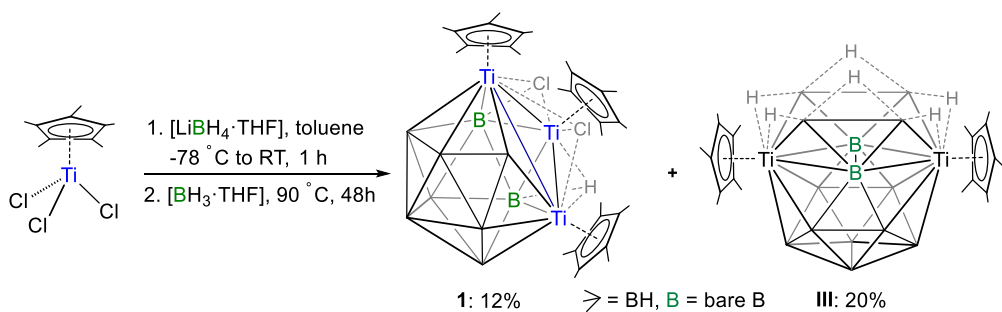
Table S8	TD-DFT calculated energies (excitation energy (eV), λ_{calc} (nm)), oscillator strength (f), and main composition of the first UV-vis electronic excitations for 3a . Experimental absorption wavelengths (λ_{exp} , nm) of 3a are given for comparison.	S39
Figure S54	Selected molecular orbitals of 3a related to most intense electronic transitions.	S40
Figure S55	Absorption spectrum of 3b computed at TD-DFT-B3LYP/Def2-SVP level of theory.	S40
Table S9	TD-DFT calculated energies (excitation energy (eV), λ_{calc} (nm)), oscillator strength (f), and main composition of the first UV-vis electronic excitations for 3b . Experimental absorption wavelengths (λ_{exp} , nm) of 3b are given for comparison.	S41
Figure S56	Selected molecular orbitals of 3b related to most intense electronic transitions.	S42
III	Cartesian Coordinates of all Optimized Structures	
Figure S57	Optimized geometry of 1 .	S43
Figure S58	Optimized geometry of 2 .	S44
Figure S59	Optimized geometry of 3a .	S45
Figure S60	Optimized geometry of 3b .	S46
IV	References	S48

I Experimental Details

General Procedures and Instrumentation

All the manipulations were conducted under an Ar/N₂ atmosphere using standard Schlenk line techniques or in a glove box. Hexane, THF, and toluene solvents were distilled from purple solutions of benzophenone ketyl. Dichloromethane and CDCl₃ were distilled from calcium hydride prior to use. [Cp^{*}TiCl₃]^[1] and Li[BH₃(EPH)]^[2,3] (E = Se and Te) were synthesized according to the literature methods, while LiBH₄ (2.0 M in THF) and [Ph₂E₂] (E = Se and Te) were used as received (Sigma Aldrich). Thin layer chromatography (TLC) was carried out on 250-μm diameter aluminum-supported silica gel TLC plates (MERCK TLC Plates) to separate the reaction mixtures. NMR spectra were recorded on a Bruker Avance III 500 MHz spectrometer. The residual solvent protons (CDCl₃, δ = 7.26 ppm) and carbon (CDCl₃, δ = 77.1 ppm) were employed as a reference for the ¹H and ¹³C{¹H} NMR spectra, respectively. The ⁷⁷Se NMR chemical shifts are referenced with Se₂Ph₂ (δ = 463 ppm in CDCl₃). The ¹¹B decoupled ¹H spectrum was obtained with inverse gated decoupling (zgig) and power gated decoupling (zgpr) pulse sequences, respectively. ¹¹B{¹H} NMR spectra were processed with a backward linear prediction algorithm to eliminate the broad ¹¹B background signal of the NMR tube.^[4] All pulse sequences are available in a commercial Bruker spectrometer. Electrospray mass (ESI-MS) spectrometric data were obtained on a Qtof Micro YA263 HRMS and 6545 Qtof LC/MS instrument. Infrared (IR) spectra of liquid samples (prepared in dichloromethane) were recorded on a JASCO FT/IR-1400 spectrometer. UV-vis spectra were recorded in dichloromethane on a Thermo Scientific (Evolution 300) UV-vis spectrometer.

Synthesis of 1: In a flame-dried Schlenk tube, [(Cp^{*}TiCl₃)] (0.100 g, 0.35 mmol) was suspended in 10 mL dry toluene and it was charged with lithium borohydride solution 2.0 M in THF (0.6 mL, 1.2 mmol) dropwise at -78 °C and kept under constant stirring for 1 h. To this in situ generated intermediate, an excess amount of [BH₃·THF] (2.5 mL, 2.5 mmol) was added and kept at 90 °C for 48 h under stirring conditions. After the addition of [BH₃·THF], the mixture becomes light green. Further, during thermolysis, the reaction mixture slowly converted to brown from light green and, after 48 h, changed to dark brown. After the completion of the reaction, the solvent was removed under vacuum. The residue was extracted with hexane/dichloromethane mixture (70:30 v/v) through a frit using 3 cm celite. The filtrate was concentrated, and the residue was subjected to chromatographic workup on 250-μm diameter aluminium-supported silica gel TLC plates (MERCK TLC Plates). Note that we have done the chromatographic workup using TLC plates inside beakers which were filled with Ar before and after filling with properly distilled eluting solvents. Elution with a hexane/dichloromethane (70:30 v/v) mixture yielded dark green **1** (0.010 g, 12%) along with previously reported open 16-vertex *oblate-hypo*-titanaborane cluster [(Cp^{*}Ti)₂B₁₄H₁₈]^[5] (**III**) (0.019 g, 20%).

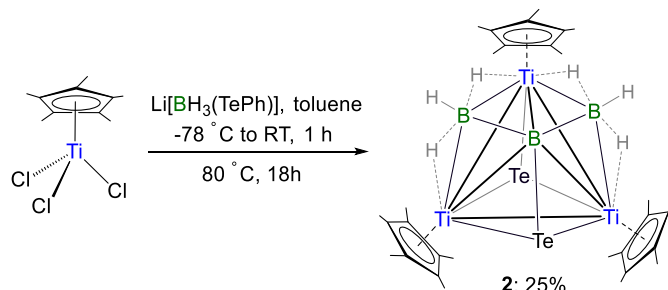


Scheme S1. Synthesis of **1**.

1: MS (ESI⁺): *m/z* calculated for [C₃₀H₅₃B₉Cl₂Ti₃ + H]⁺: 726.2956, found: 726.3257; ¹¹B{¹H} NMR (160 MHz, CDCl₃, 22 °C): δ = 31.6 (br, 4B), 40.2 (br, 2B), 45.0 (br, 1B), 52.3 (br, 1B), 66.4 (br, 1B) ppm; ¹¹B NMR (160 MHz, CDCl₃, 22 °C): δ = 31.6 (d, ¹J_{B-H} = 125 Hz, 4B), 40.3 (d, ¹J_{B-H} = 127 Hz, 2B), 45.1 (d, ¹J_{B-H} = 103 Hz, 1B), 52.3 (br, 1B), 66.4 (br, 1B) ppm; ¹H NMR (500 MHz,

CDCl_3 , 22 °C): $\delta = -5.67$ (br, 1H, Ti-H-B), 2.03 (s, 30H, 2Cp*), 2.05 (s, 15H, 1Cp*), 3.53 (br, B-Ht), 7.00 (br, B-Ht), 7.15 (br, B-Ht) ppm; $^{13}\text{C}\{\text{H}\}$ NMR (125 MHz, CDCl_3 , 22 °C): $\delta = 13.3$ and 13.8 (C_5Me_5), 118.9 and 125.1 (C_5Me_5), ppm; IR (KBr, cm^{-1}): $\bar{\nu} = 2959, 2921, 2852, 2544$ (B-H_t), 1737, 1652, 1462, 1378, 1262, 1094, 1019, 865, 804, 741, 706; UV-Vis (CH_2Cl_2): $\lambda = 230, 252, 455, 607$ nm.

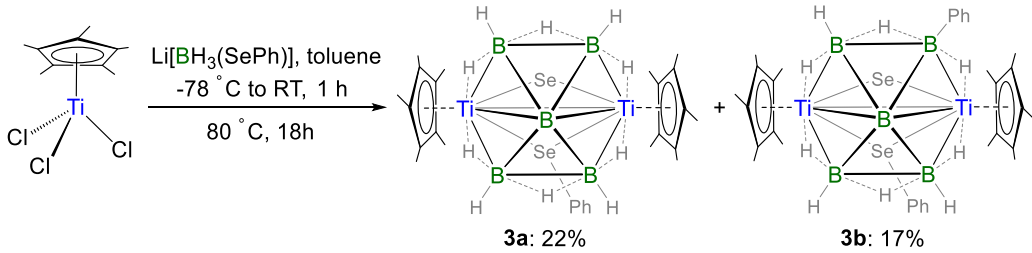
Synthesis of 2: In a flame-dried Schlenk tube, $[(\text{Cp}^*\text{TiCl}_3)]$ (0.100 g, 0.35 mmol) was suspended in 10 mL dry toluene and chilled to -78 °C. Then, a freshly prepared toluene solution of $\text{Li}[\text{BH}_3\text{TePh}]$ (3 equivalents, 1.05 mmol, in 10 mL) was transferred to it through a cannula. The reaction mixture was allowed to come to room temperature over 1 hour under stirring and thermolyzed at 80 °C for 18 h. After 1 hour, the mixture becomes brown and, after 18 h, changes to dark brown. After the completion of the reaction, the solvent was removed under vacuum. The residue was extracted with hexane/dichloromethane mixture (80:20 v/v) through a frit using 3 cm celite. The filtrate was concentrated, and the residue was subjected to chromatographic workup on 250-μm diameter aluminium-supported silica gel TLC plates (MERCK TLC Plates). Elution with a hexane/dichloromethane (80:20 v/v) mixture yielded yellow **2** (0.024 g, 25%) along with a few unidentified air and moisture-sensitive products in low yields.



Scheme S2. Synthesis of **2**.

2: MS (ESI⁺): m/z calculated for $[\text{C}_{30}\text{H}_{51}\text{B}_3\text{Te}_2\text{Ti}_3 + \text{H}]^+$: 845.0926, found: 845.1155; $^{11}\text{B}\{\text{H}\}$ NMR (160 MHz, CDCl_3 , 22 °C): $\delta = -7.7$ (br, 2B, BH₃), 54.0 (br, 1B, bare B) ppm; ^1H NMR (500 MHz, CDCl_3 , 22 °C): $\delta = -2.79$ (br, 4H, Ti-H-B), 2.04 (s, 15H, 1Cp*), 2.09 (s, 30H, 2Cp*), 2.36 (br, 2B, B-Ht) ppm; $^1\text{H}\{^{11}\text{B}\}$ NMR (500 MHz, CDCl_3 , 22 °C): $\delta = -2.80$ (br, 4H, Ti-H-B), 2.04 (s, 15H, 1Cp*), 2.09 (s, 30H, 2Cp*), 2.39 (br, 2B, B-Ht) ppm; IR (KBr, cm^{-1}): $\bar{\nu} = 2959, 2925, 2871, 2492$ (B-H_t), 2083 (B-H_b), 1648, 1452, 1378, 1259, 1094, 1063, 1021, 801, 738, 697; UV-Vis (CH_2Cl_2): $\lambda = 230, 264, 346$ nm.

Synthesis of 3a and 3b: In a flame-dried Schlenk tube, $[(\text{Cp}^*\text{TiCl}_3)]$ (0.100 g, 0.35 mmol) was suspended in 10 mL dry toluene and chilled to -78 °C. Then, a freshly prepared toluene solution of $\text{Li}[\text{BH}_3\text{SePh}]$ (3 equivalents, 1.05 mmol, in 10 mL) was transferred to it through a cannula. The reaction mixture was allowed to come to room temperature over 1 hour under stirring and thermolyzed at 80 °C for 18 h. After 1 h, the mixture becomes brown and, after 18 h, changes to dark brown. After the completion of the reaction, the solvent was removed under vacuum. The residue was extracted with hexane/dichloromethane mixture (80:20 v/v) through a frit using 3 cm celite. The filtrate was concentrated, and the residue was subjected to chromatographic workup on 250-μm diameter aluminium-supported silica gel TLC plates (MERCK TLC Plates). Elution with a hexane/dichloromethane (80:20 v/v) mixture yielded yellow **3a** (0.025 g, 22%) and yellow **3b** (0.022 g, 17%).



Scheme S3. Synthesis of **3a** and **3b**.

3a: MS (ESI $^+$): m/z calculated for $[\text{C}_{26}\text{H}_{45}\text{B}_5\text{Se}_2\text{Ti}_2 - \text{BH}_2]^+$: 653.1080, found: 653.1082; $^{11}\text{B}\{\text{H}\}$ NMR (160 MHz, CDCl_3 , 22 °C): $\delta = -2.2$ (br, 2B, BH_3), 0.8 (br, 2B, BH_3), 51.3 (br, 1B, bare B) ppm; ^{11}B NMR (160 MHz, CDCl_3 , 22 °C): $\delta = -2.4$ (br, 2B, BH_3), 0.4 (br, 2B, BH_3), 51.3 (br, 1B, bare B) ppm; ^1H NMR (500 MHz, CDCl_3 , 22 °C): $\delta = -2.34$ (br, 1H, Ti-H-B), -1.73 (br, 2H, Ti-H-B), -0.77 (br, 1H, Ti-H-B), -0.54 (br, 2H, B-H-B), 2.01 (br, 2H, B-Ht), 2.23 (s, 30H, 2Cp*), 2.94 (br, 2H, B-Ht), 7.28-7.56 (m, 5H, Ph) ppm; $^1\text{H}\{^{11}\text{B}\}$ NMR (500 MHz, CDCl_3 , 22 °C): $\delta = -2.35$ (br, 1H, Ti-H-B), -1.75 (br, 2H, Ti-H-B), -0.79 (br, 1H, Ti-H-B), -0.54 (br, 2H, B-H-B), 1.87 (br, 2H, B-Ht), 2.23 (s, 30H, 2Cp*), 2.72 (br, 2H, B-Ht), 7.28-7.56 (m, 5H, Ph) ppm; $^{13}\text{C}\{\text{H}\}$ NMR (125 MHz, CDCl_3 , 22 °C): $\delta = 14.1$ (C_5Me_5), 123.0 (C_5Me_5), 127.7-133.2 (C_6H_5) ppm; ^{77}Se NMR (95 MHz, CDCl_3 , 22 °C): $\delta = 346.9$ ($\mu\text{-Se}$), 527.3 ($\mu\text{-SePh}$) ppm; IR (KBr, cm^{-1}): $\bar{\nu} = 2961, 2921, 2852, 2503$ (B-H_t), 2124 (B-H_b), 1645, 1473, 1432, 1128, 1092, 1065, 1019, 799, 731, 688; UV-Vis (CH_2Cl_2): $\lambda = 230, 248, 276, 364$ nm.

3b: MS (ESI $^+$): m/z calculated for $[\text{C}_{32}\text{H}_{49}\text{B}_5\text{Se}_2\text{Ti}_2]^+$: 742.1651, found: 742.1716; $^{11}\text{B}\{\text{H}\}$ NMR (160 MHz, CDCl_3 , 22 °C): $\delta = -0.3$ (br, 1B, BH_3), 1.4 (br, 2B, BH_3), 5.2 (br, 1B, BH_2Ph), 50.6 (br, 1B, bare B) ppm; ^{11}B NMR (160 MHz, CDCl_3 , 22 °C): $\delta = 1.3$ (br, 3B, BH_3), 5.3 (br, 1B, BH_2Ph), 50.6 (br, 1B, bare B) ppm; ^1H NMR (500 MHz, CDCl_3 , 22 °C): $\delta = -1.62$ (br, 1H, Ti-H-B), -1.08 (br, 1H, Ti-H-B), -0.59 (br, 2H, Ti-H-B), -0.19 (br, 2H, B-H-B), 1.92 (br, 2H, B-Ht), 2.14 (s, 15H, 1Cp*), 2.23 (s, 15H, 1Cp*), 3.20 (br, 2H, B-Ht), 7.06-7.59 (m, 10H, Ph) ppm; $^1\text{H}\{^{11}\text{B}\}$ NMR (500 MHz, CDCl_3 , 22 °C): $\delta = -1.62$ (br, 1H, Ti-H-B), -1.08 (br, 1H, Ti-H-B), -0.59 (br, 2H, Ti-H-B), -0.26 (br, 1H, B-H-B), -0.14 (br, 1H, B-H-B), 1.93 (br, 2H, B-Ht), 2.14 (s, 15H, 1Cp*), 2.23 (s, 15H, 1Cp*), 3.10 (br, 2H, B-Ht), 7.05-7.59 (m, 10H, Ph) ppm; $^{13}\text{C}\{\text{H}\}$ NMR (125 MHz, CDCl_3 , 22 °C): $\delta = 14.1$ and 14.2 ($2\text{C}_5\text{Me}_5$), 122.9 and 123.0 ($2\text{C}_5\text{Me}_5$), 126.9-135.1 ($2\text{C}_6\text{H}_5$) ppm; ^{77}Se NMR (95 MHz, CDCl_3 , 22 °C): $\delta = 293.7$ ($\mu\text{-Se}$), 540.5 ($\mu\text{-SePh}$) ppm; IR (KBr, cm^{-1}): $\bar{\nu} = 2963, 2929, 2854, 2500$ (B-H_t), 2088 (B-H_b), 1643, 1262, 1094, 1021, 867, 799, 692; UV-Vis (CH_2Cl_2): $\lambda = 230, 250, 269, 317, 366$ nm.

I.1 UV-visible Studies

In order to investigate the optical properties of these coloured metallaborane clusters **1**, **2**, **3a**, and **3b**, we have carried out UV-vis study in CH_2Cl_2 solution. The UV-vis absorption spectra of all the complexes were measured in the range of 200-800 nm in CH_2Cl_2 solution at 298 K (Figures S38). All of them display the most intense peaks at higher energy regions 230-276 nm due to the $\pi-\pi^*$ transition of Cp* ligands, characteristic bands for most Cp* based metal complexes.^[6] The absorptions with $\lambda > 300$ nm exhibit mainly two to three absorption bands. These comparatively low energy bands, around 317-607 nm, have been assigned to the charge transfer bands.^[7-9] To reproduce the UV-vis spectrum and get some idea about the electronic transitions, Time-Dependent DFT formalism was used (Figures S49-S56, Tables S6-S9). The studies show that the absorption in the range of 317-607 nm may be assigned to the electronic transitions that correspond to electron density flow from the boron moieties or chalcogen atoms to the metal centers.

I.2 Supplementary Data

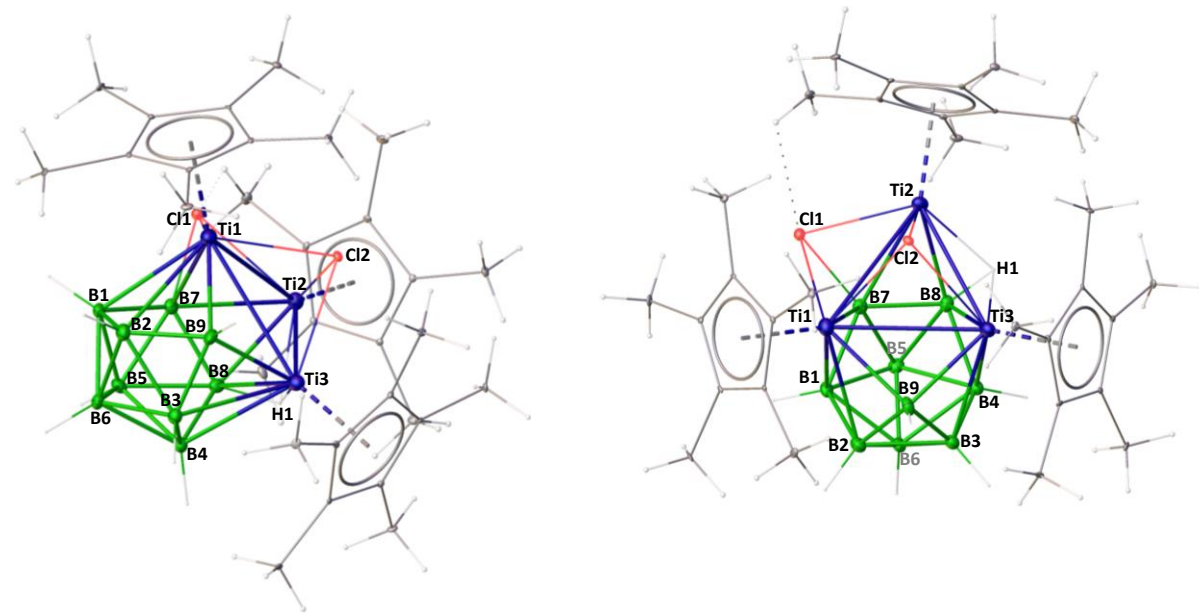


Figure S1. Molecular structure and labelling diagram of **1**. Side view (left); top view (right). Selected bond lengths (\AA) and bond angles ($^\circ$): Ti-Ti3 3.073(3), Ti1-B1 2.513(16), Ti1-B9 2.174(15), B2-B9 1.61(2), B7-Cl1 1.854(19), Ti1-Cl1 2.543(5), B8-H1 1.19(3), Ti2-H1 1.95(13), Ti1-Ti2-Ti3 58.01(7), Ti1-B9-Ti3 91.3(6).

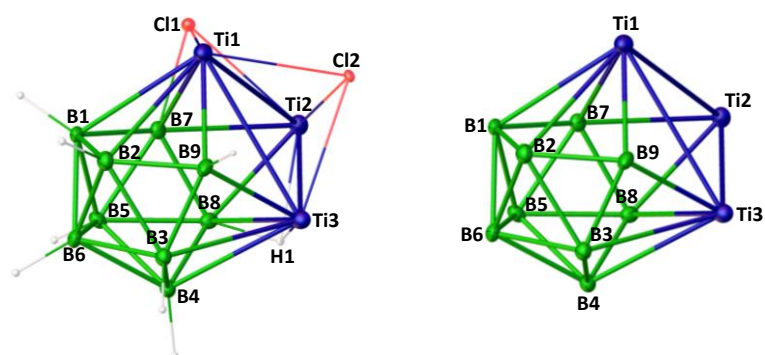


Figure S2. Icosahedron core [Ti₃B₉] of **1** with bridging ligands (left) and icosahedron core [Ti₃B₉] of **1** (right).

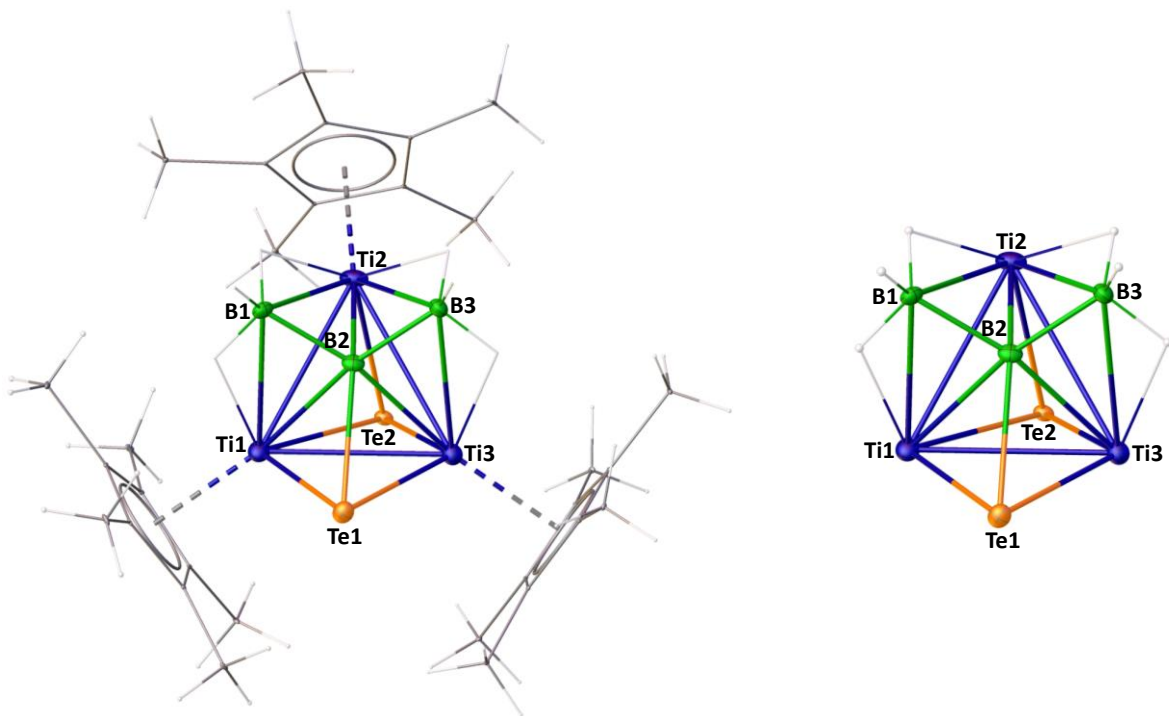


Figure S3. Molecular structure and labelling diagram of **2** (left). Selected bond lengths (\AA) and angles ($^\circ$) in **2**: Ti-Ti3 3.073(3), Ti1-B1 2.513(16), Ti1-B9 2.174(15), B2-B9 1.61(2), B7-Cl1 1.854(19), Ti1-Cl1 2.543(5), B8-H1 1.19(3), Ti2-H1 1.95(13), Ti1-Ti2-Ti3 58.01(7), Ti1-B9-Ti3 91.3(6). Tetracapped tetrahedron $[\text{Ti}_3\text{B}_3\text{Te}_2]$ core of **1** with bridging ligands (right).

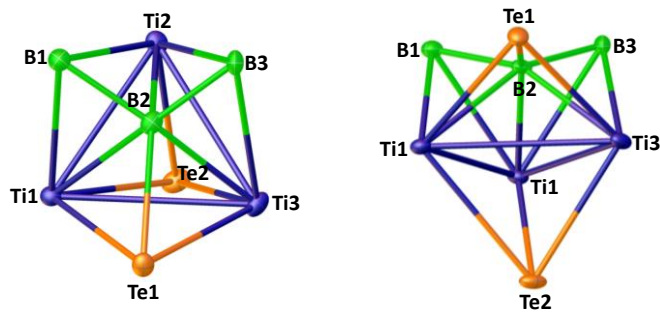


Figure S4. Tetracapped tetrahedron $[\text{Ti}_3\text{B}_3\text{Te}_2]$ core of **2**. Side view (left); top view (right).

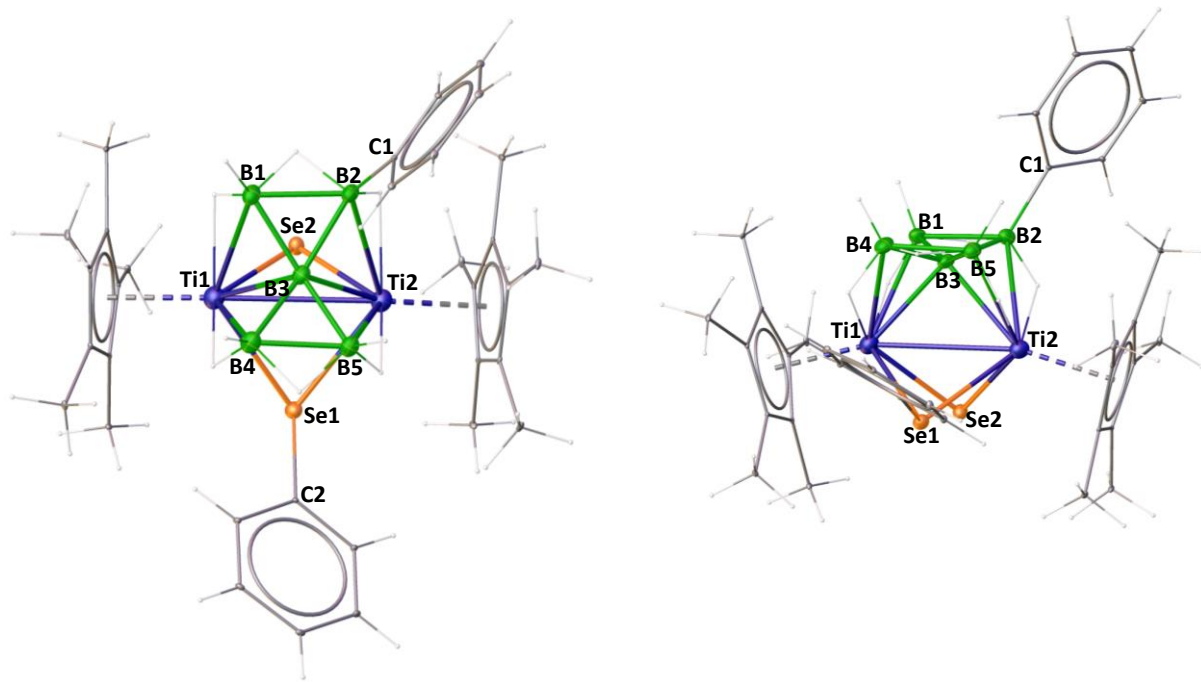


Figure S5. Molecular structure and labelling diagram of **3b**. Side view (left); top view (right). Selected bond lengths (\AA) and bond angles ($^\circ$): Ti1-Ti2 3.0281(7), Ti1-B3 2.271(4), B1-B2 1.784(5), Ti1-B3-Ti2 84.03(12).

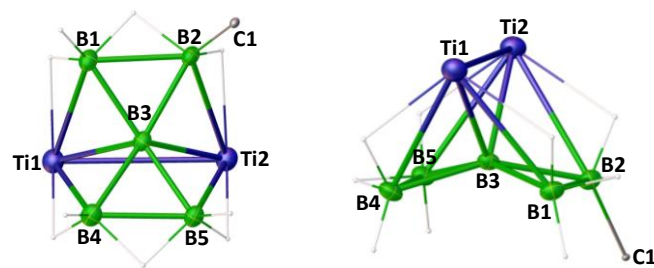
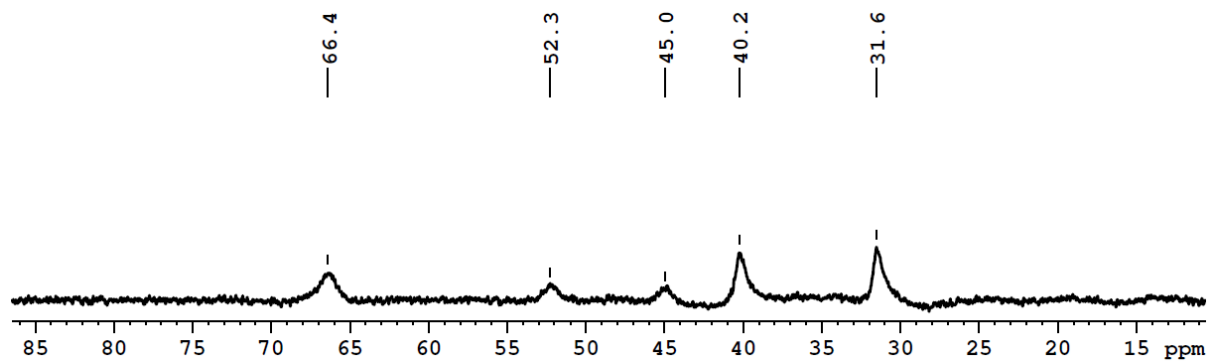
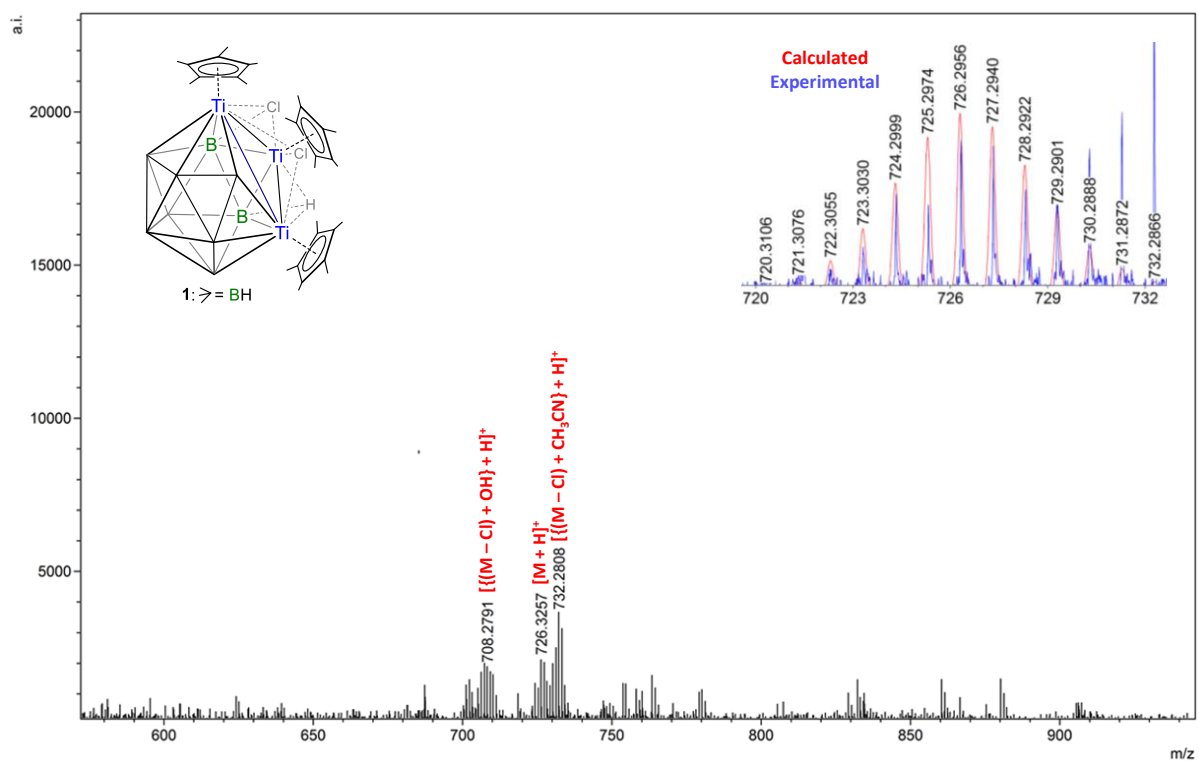


Figure S6. $[\text{Ti}_3\text{B}_3\text{Te}_2]$ core of **3b** with bridging ligands. Top view (left); side view (right).

I.3 Spectroscopic Details



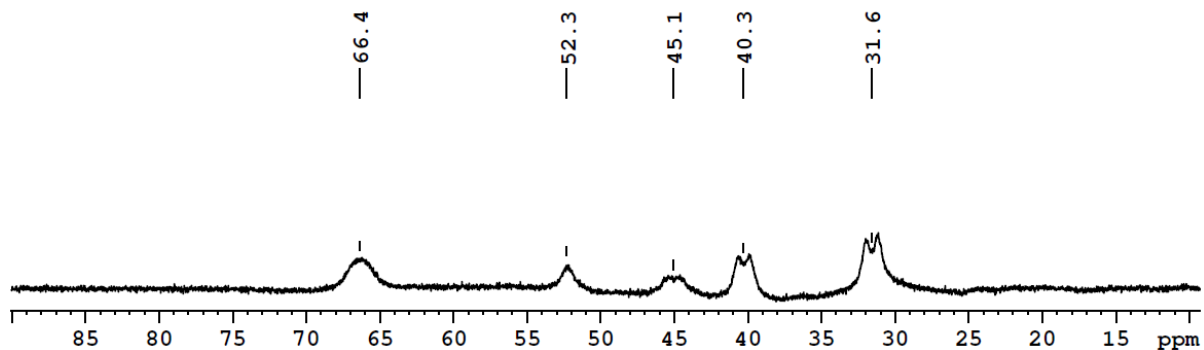


Figure S9. ^{11}B NMR spectrum of **1** in CDCl_3 .^[4] Note that the chemical shifts observed at $\delta = 31.6$ and 40.3 ppm correspond to a set of four boron atoms (B1, B2, B3, and B4; Figure S1) and two boron atoms (B5 and B6; Figure S1), respectively. These boron atoms are bound to terminal hydrogen atoms. The resonance at $\delta = 45.1$ ppm is assigned to the B8 atom, which is connected to bridging hydrogen atoms, resulting in a very weak doublet. No splitting is observed for the $\delta = 52.3$ ppm signal, as the corresponding boron atom (B7) is bonded to a chlorine atom. Additionally, the chemical shift at $\delta = 66.4$ ppm corresponds to the B9 boron atom appearing broadened, likely due to the quadrupole moment of the ^{11}B nuclei.

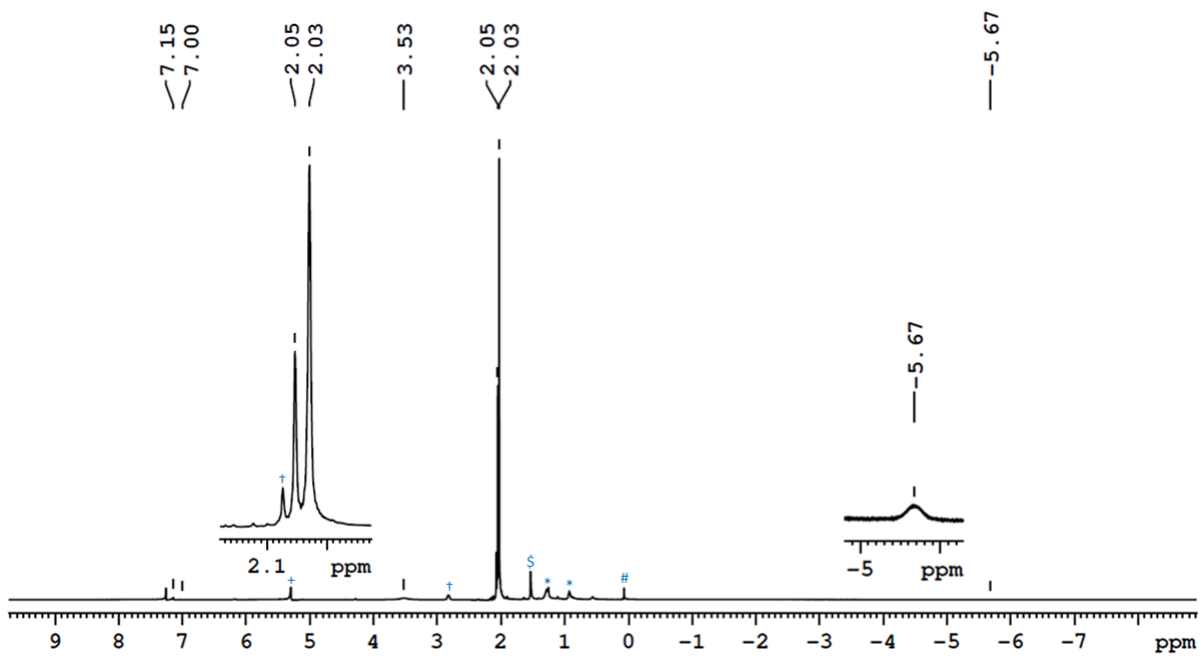


Figure S10. ^1H NMR spectrum of **1** in CDCl_3 ([†]Inseparable impurity, $\$$ H_2O , *Grease, #Silicon grease).

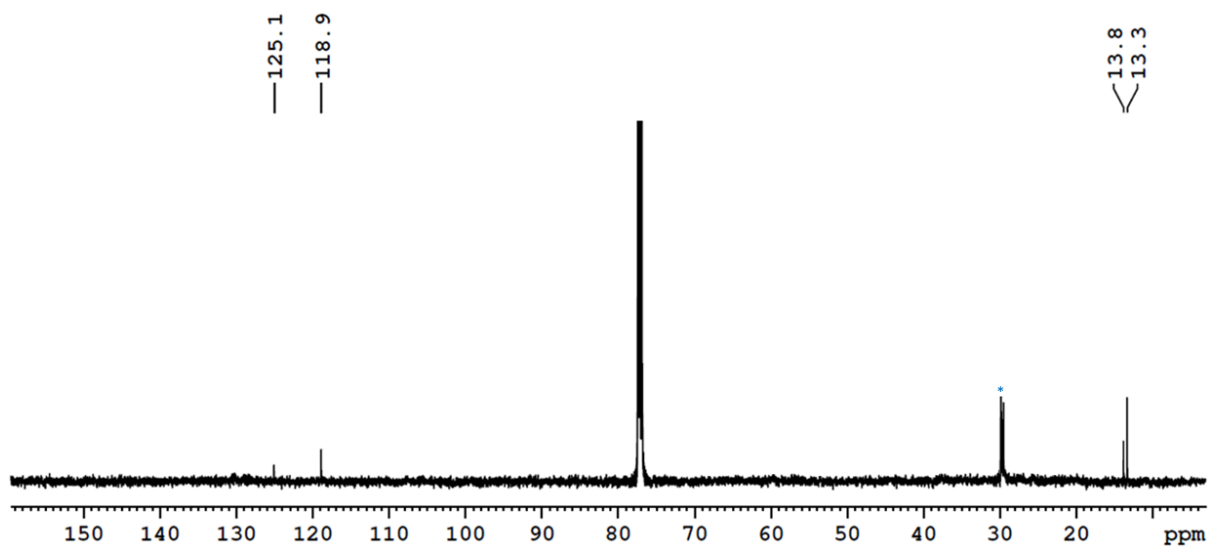


Figure S11. $^{13}\text{C}\{\text{H}\}$ NMR spectrum of **1** in CDCl_3 (*Grease).

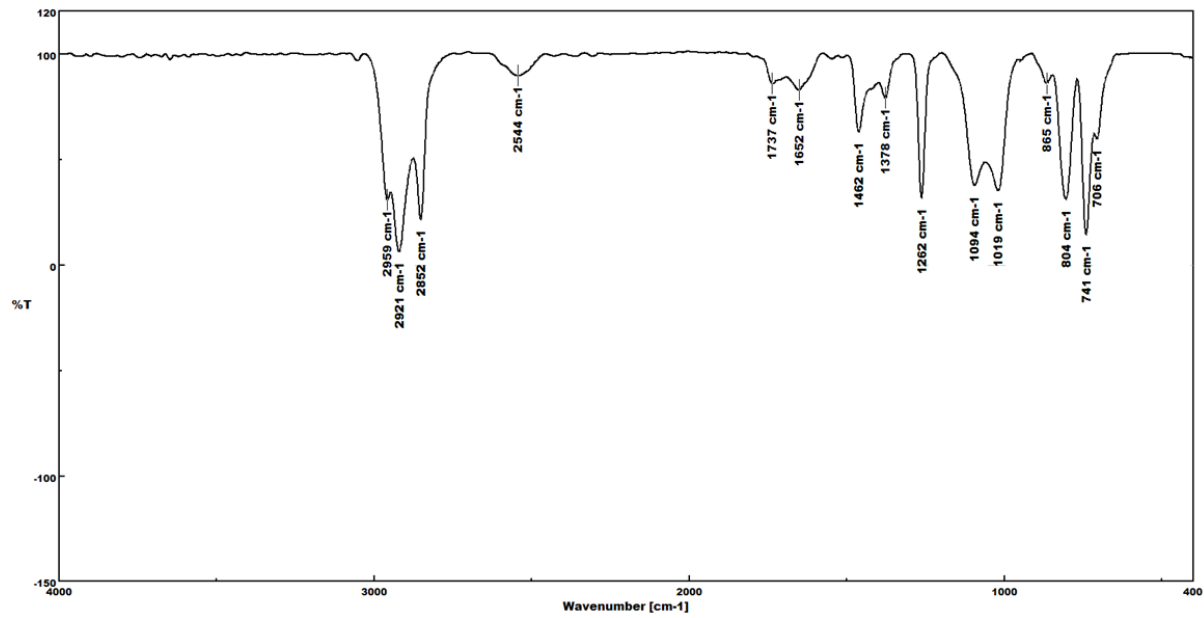


Figure S12. IR spectrum of **1**.

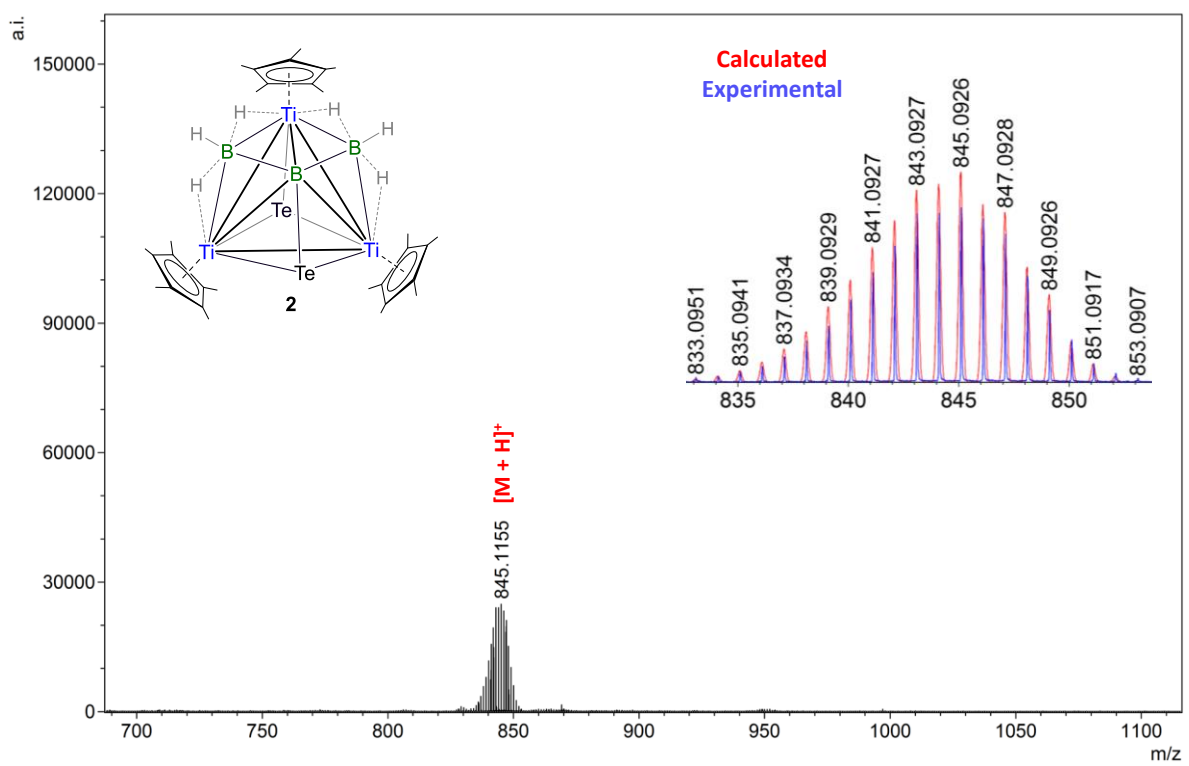


Figure S13. ESI-MS spectrum of **2**.

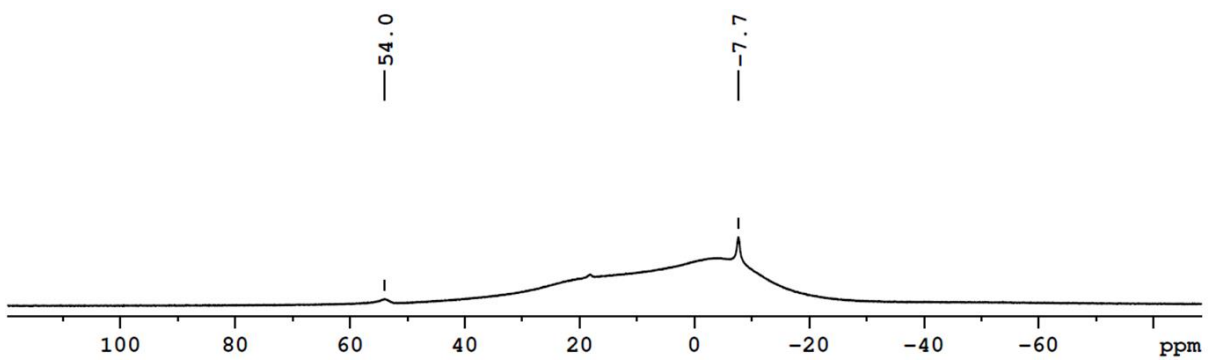


Figure S14. $^{11}\text{B}\{^1\text{H}\}$ NMR spectrum of **2** in CDCl_3 .

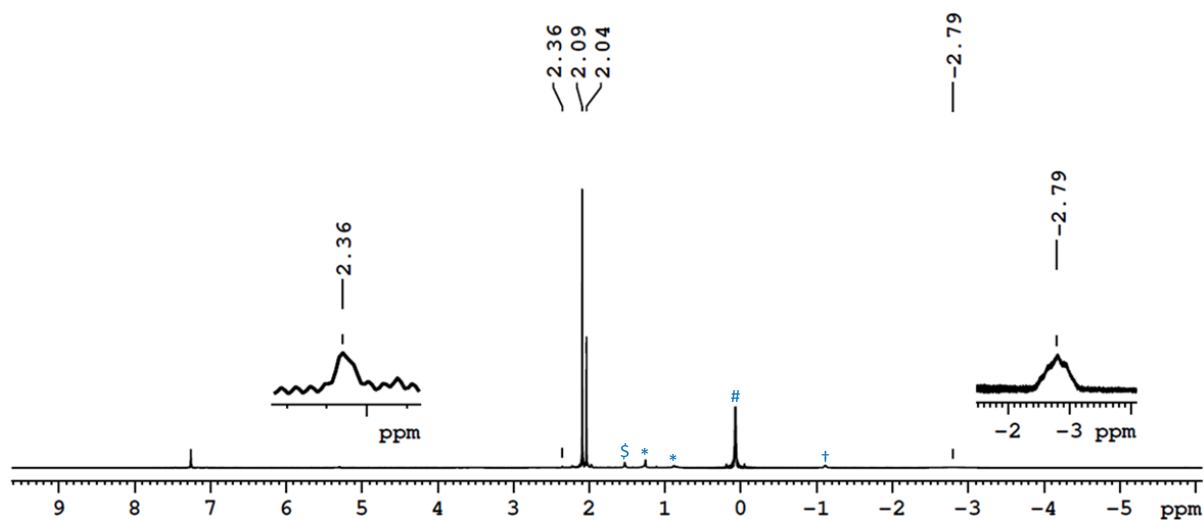


Figure S15. ^1H NMR spectrum of **2** in CDCl_3 ($\$ \text{H}_2\text{O}$, *Grease, #Silicon grease, †Inseparable impurity).

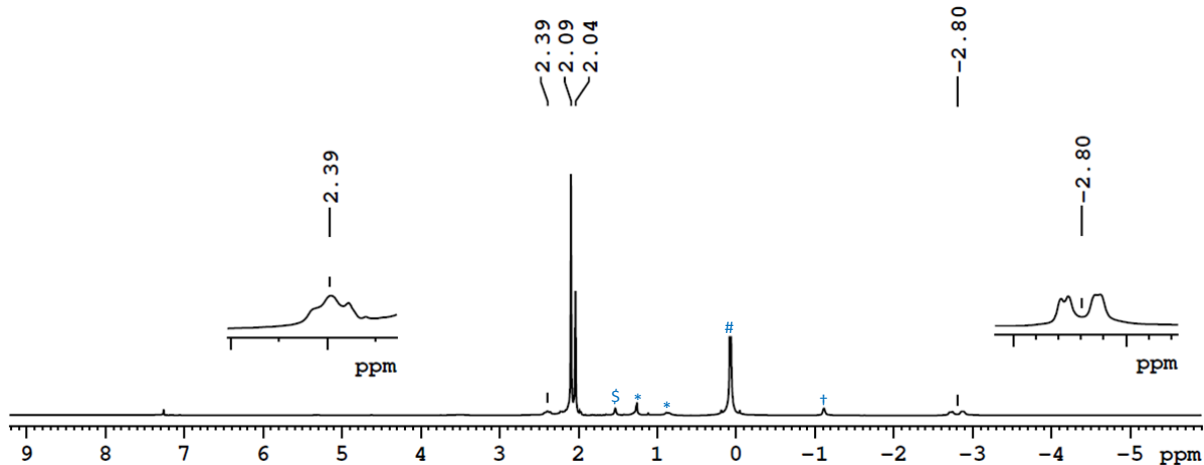


Figure S16. $^1\text{H}\{^{11}\text{B}\}$ NMR spectrum of **2** in CDCl_3 ($\$ \text{H}_2\text{O}$, *Grease, #Silicon grease, †Inseparable impurity).

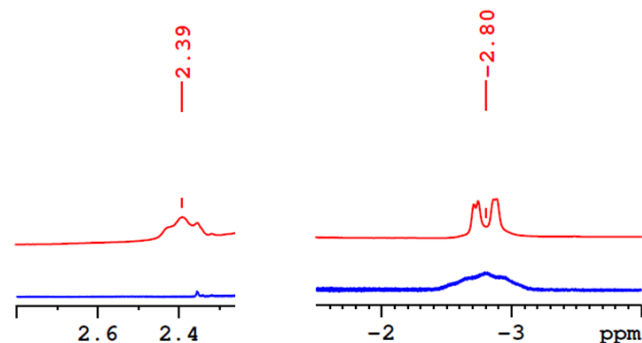


Figure S17. Stacked ^1H (bottom) and $^1\text{H}\{^{11}\text{B}\}$ NMR (top) spectra of **2** in CDCl_3 .

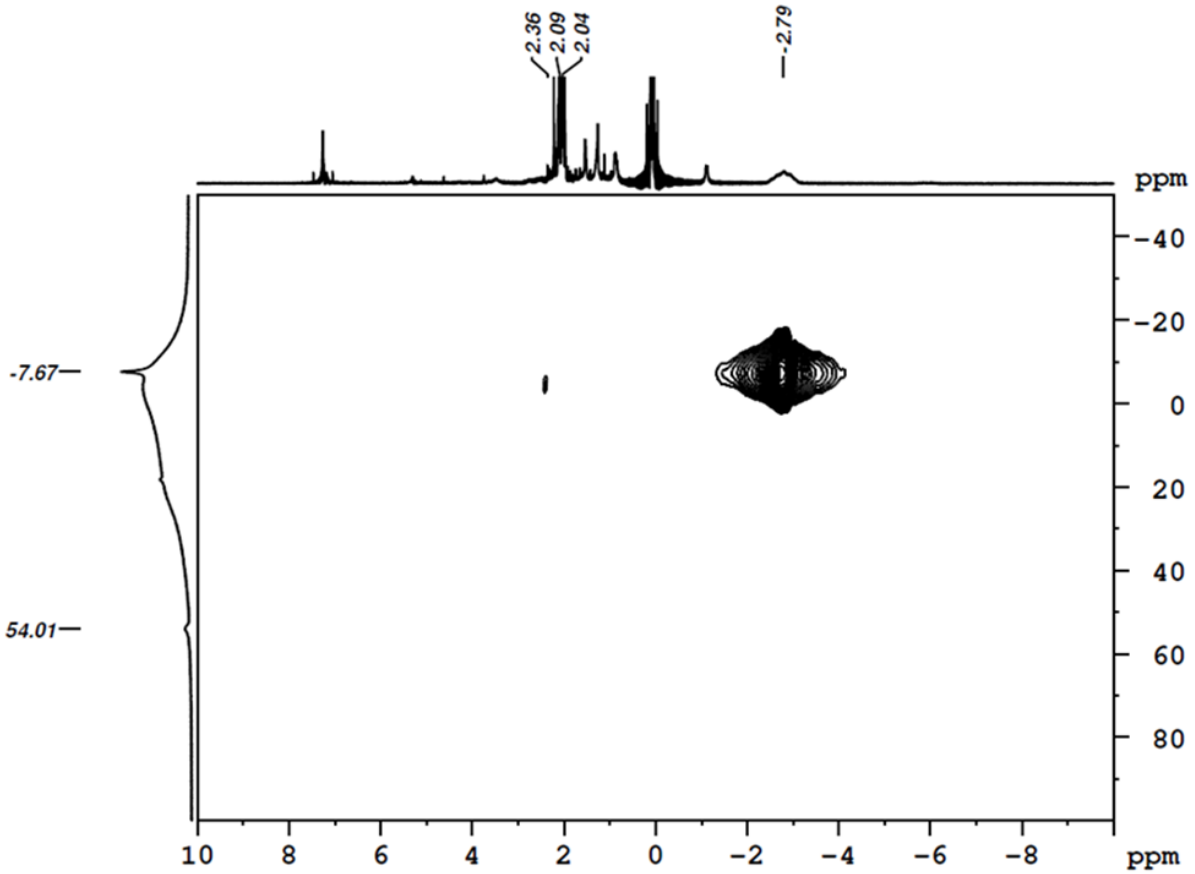


Figure S18. ^1H - ^{11}B HSQC NMR spectrum of **2** in CDCl_3 .

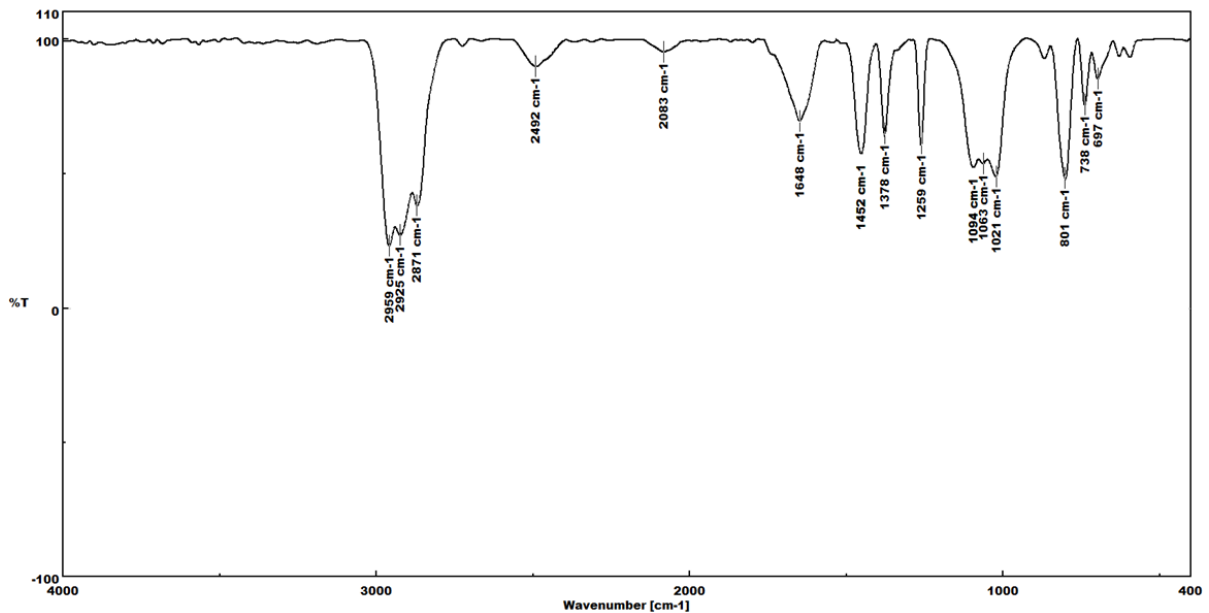


Figure S19. IR spectrum of **2**.

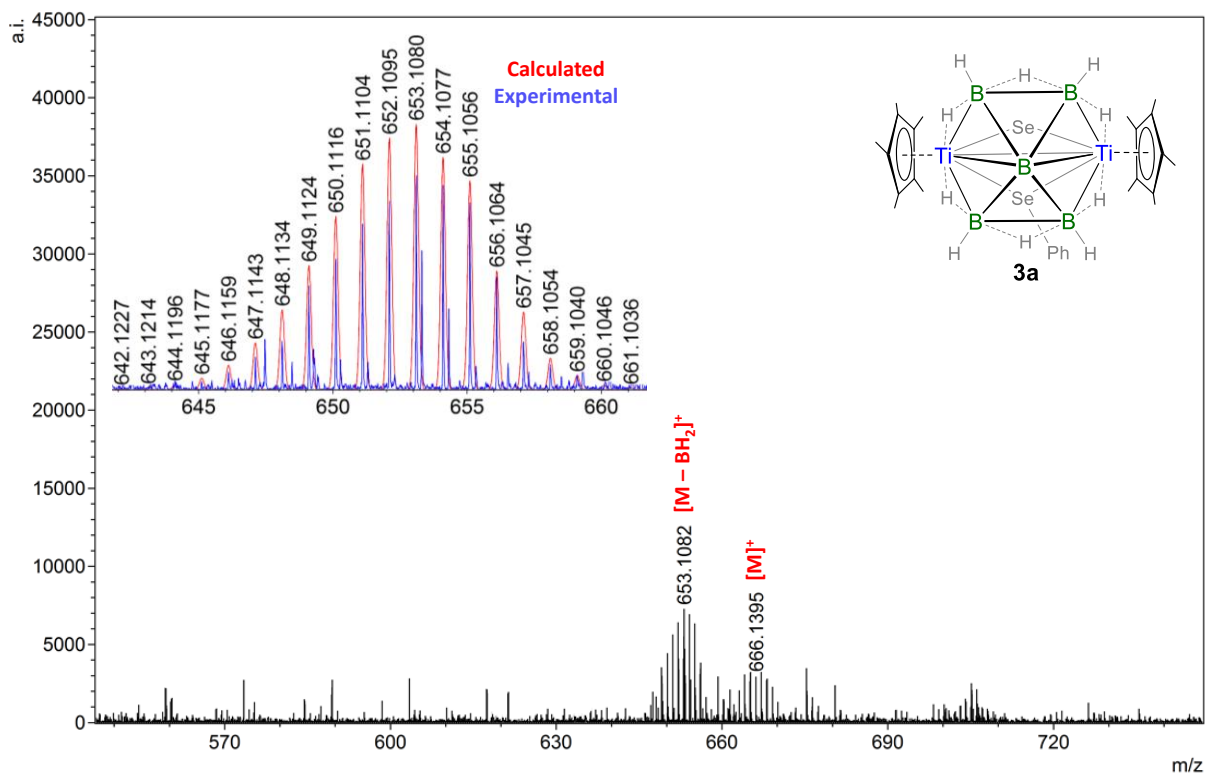


Figure S20. ESI-MS spectrum of **3a**.

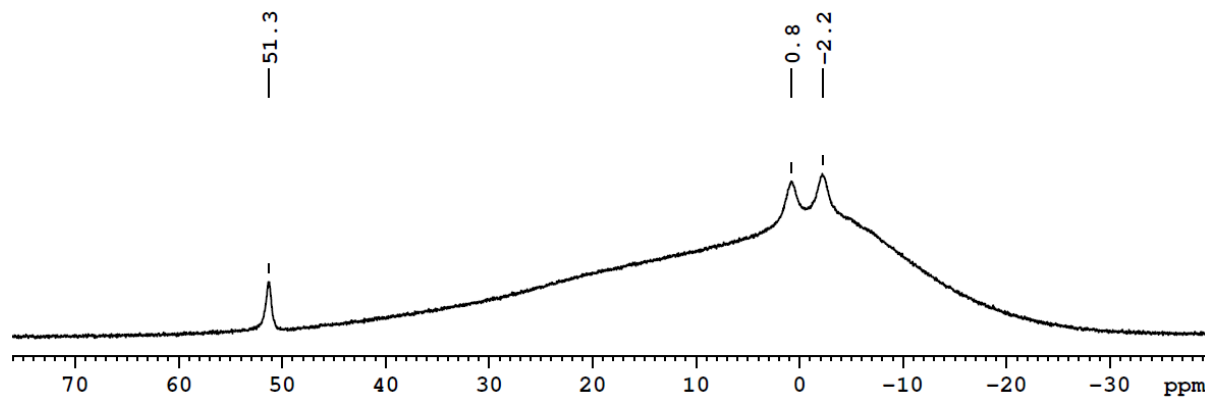


Figure S21. ¹¹B{¹H} NMR spectrum of **3a** in CDCl_3 .

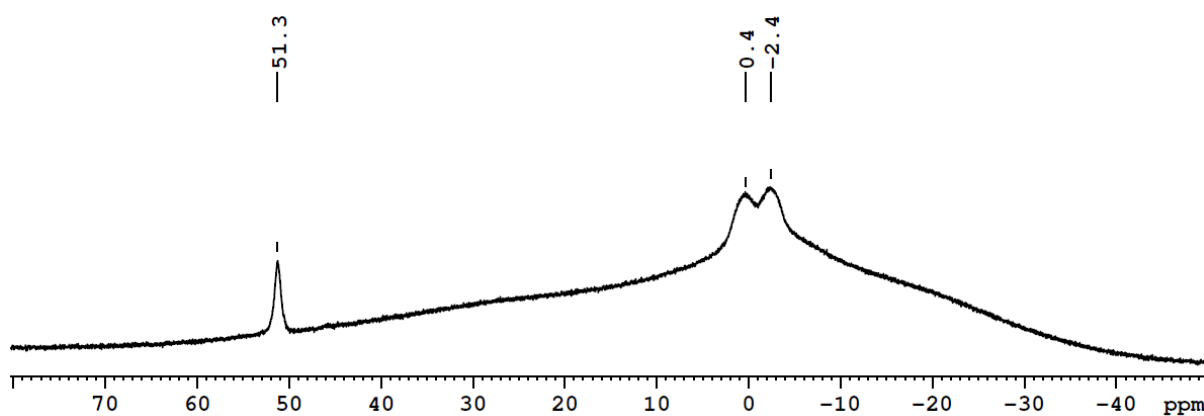


Figure S22. ^{11}B NMR spectrum of **3a** in CDCl_3 . Note that the chemical shifts observed at $\delta = -2.4$ and 0.4 ppm correspond to two sets of BH_3 boron atoms, which are bonded to the terminal and bridging hydrogen atoms (however, instead of splitting, broadened signals observed). The resonance at $\delta = 51.3$ ppm is attributed to the bare boron atom and exhibits no splitting or broadening.

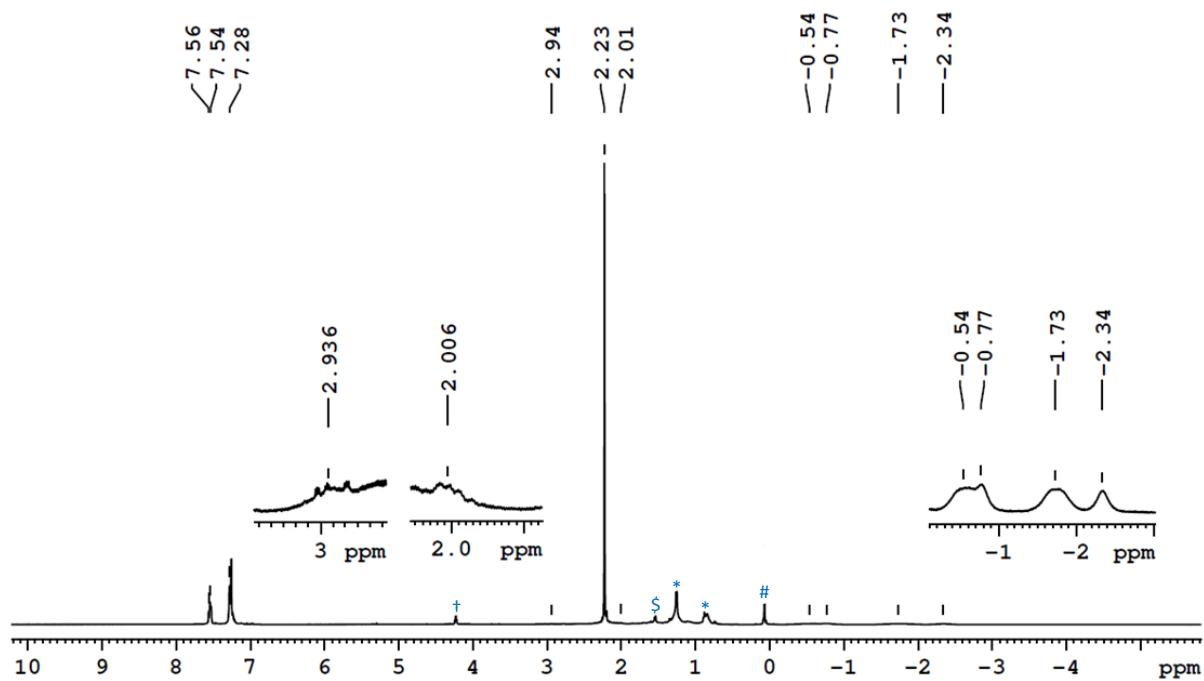


Figure S23. ^1H NMR spectrum of **3a** in CDCl_3 ([†]Inseparable impurity, ^{\$} H_2O , ^{*}Grease, [#]Silicon grease).

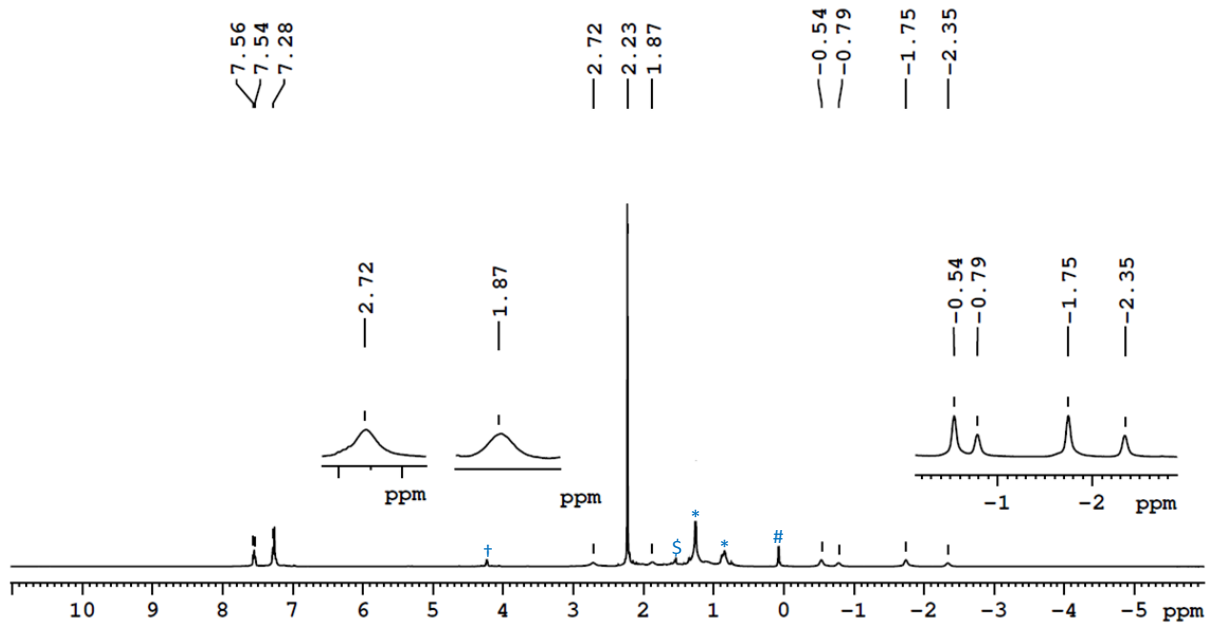


Figure S24. $^1\text{H}\{^{11}\text{B}\}$ NMR spectrum of **3a** in CDCl_3 (\ddagger Inseparable impurity, $\$$ H_2O , *Grease, #Silicon grease).

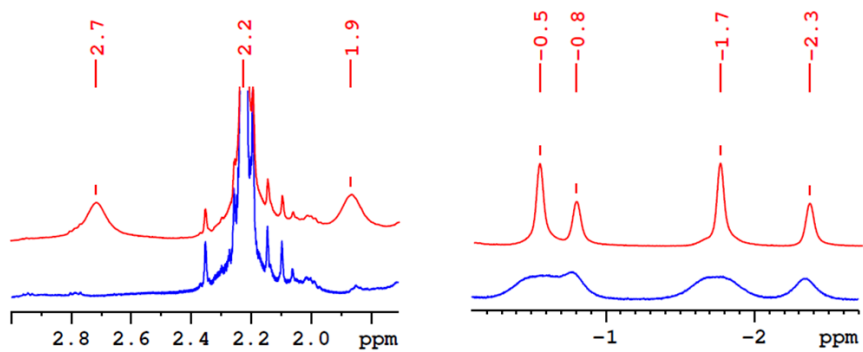


Figure S25. Stacked ^1H (bottom) and $^1\text{H}\{^{11}\text{B}\}$ NMR (top) spectra of **3a** in CDCl_3 .

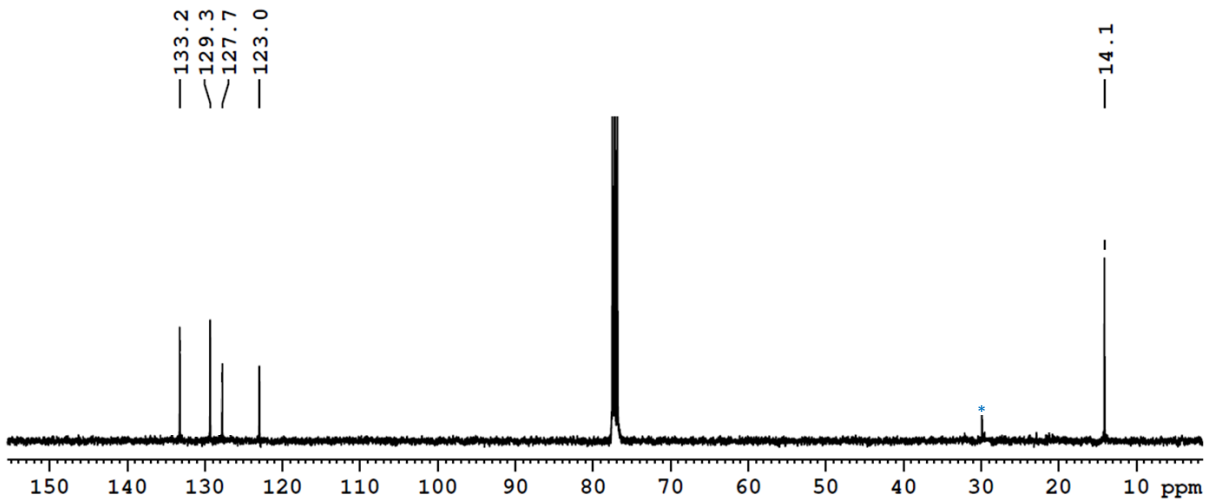


Figure S26. $^{13}\text{C}\{^1\text{H}\}$ NMR spectrum of **3a** in CDCl_3 (*Grease).

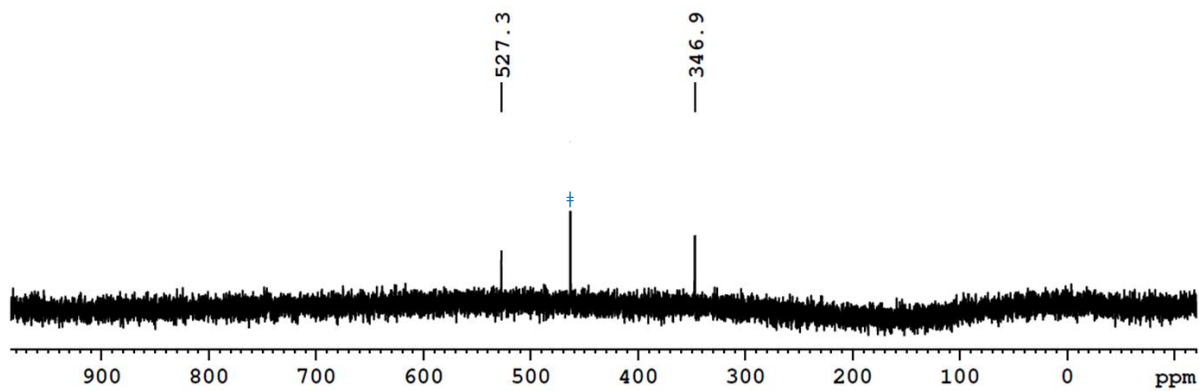


Figure S27. ⁷⁷Se NMR spectrum of **3a** in CDCl₃ (⊕ Peak at δ = 463 ppm is due to the presence of Se₂Ph₂ as external reference).

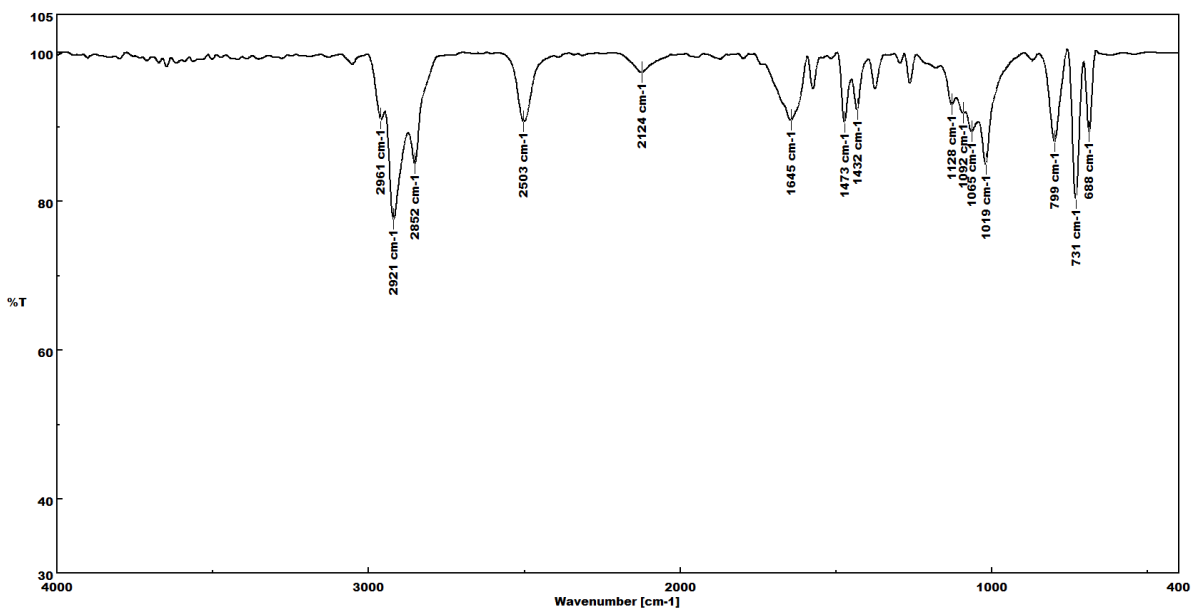


Figure S28. IR spectrum of **3a**.

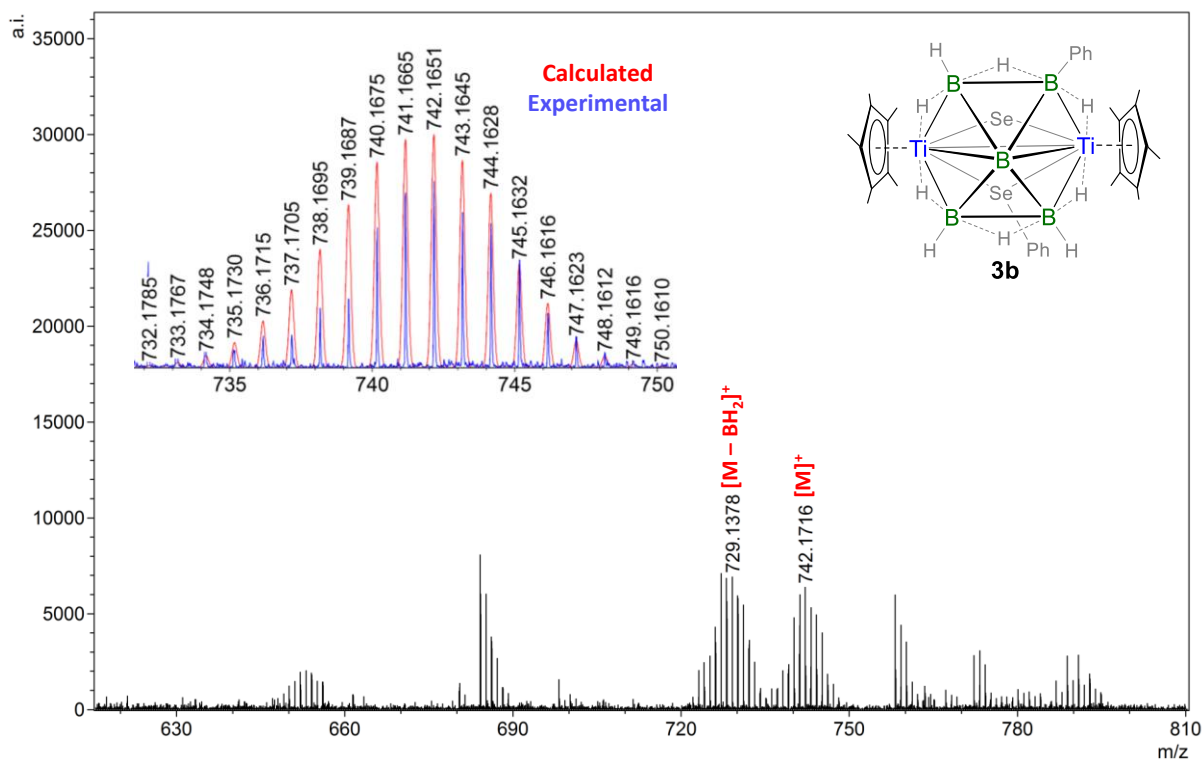


Figure S29. ESI-MS spectrum of **3b**.

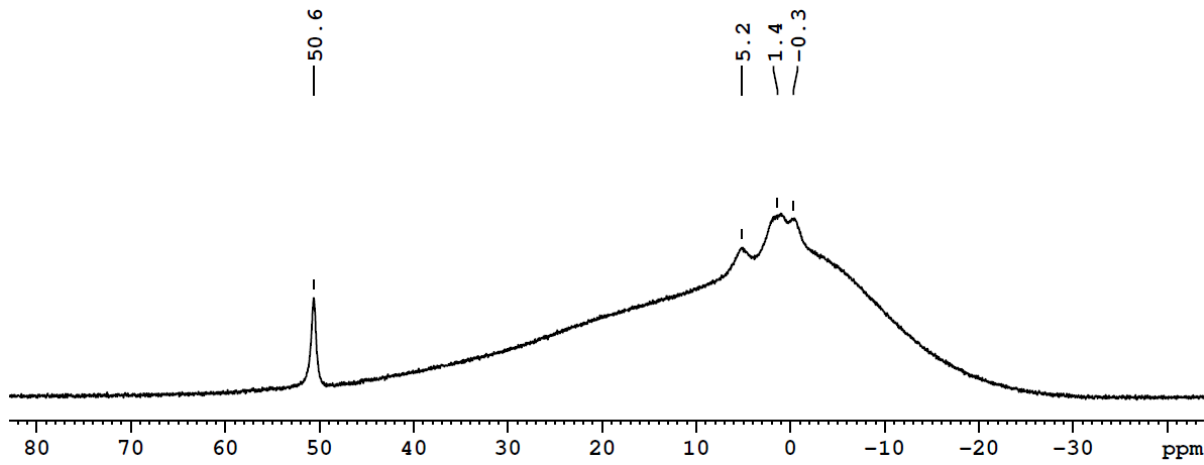


Figure S30. $^{11}\text{B}\{^1\text{H}\}$ NMR spectrum of **3b** in CDCl_3 .

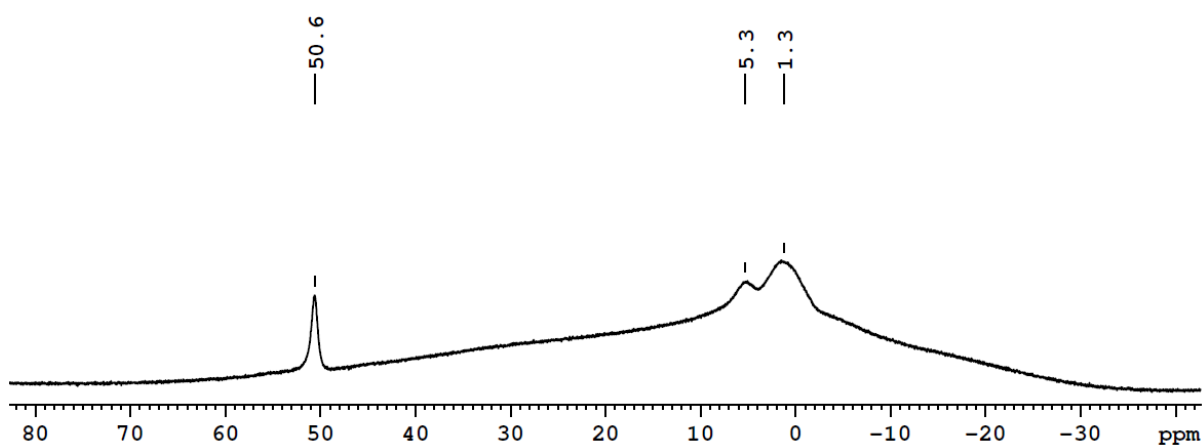


Figure S31. ^{11}B NMR spectrum of **3b** in CDCl_3 . The chemical shift observed at $\delta = 1.3$ ppm corresponds to two sets of BH_3 boron atoms bonded to the terminal and bridging hydrogen atoms. These two sets of BH_3 signals represent two inequivalent boron atoms in a 1:2 ratio in $^1\text{H}\{^{11}\text{B}\}$ NMR spectrum and appear merged in ^{11}B NMR due to the broadening of the signals. The resonance at $\delta = 5.3$ ppm is assigned to the BH_2Ph boron atom, which is connected to bridging hydrogen atoms. This signal appears broadened, likely due to the quadrupole moment of the ^{11}B nuclei. Additionally, the resonance at $\delta = 50.6$ ppm is attributed to the bare boron atom, which exhibits no splitting or broadening.

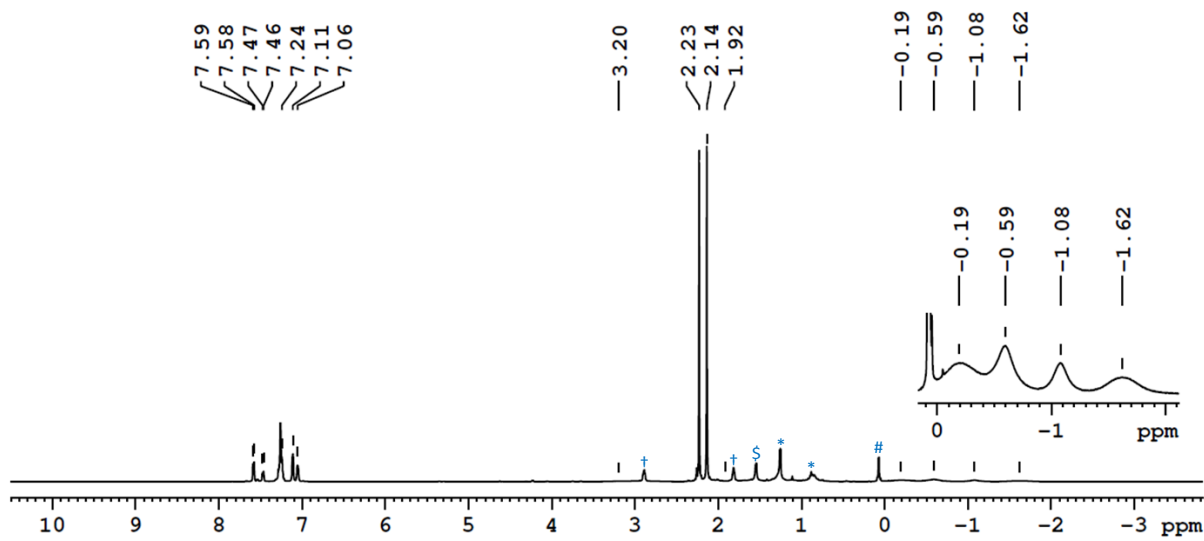


Figure S32. ^1H NMR spectrum of **3b** in CDCl_3 (\ddagger Inseparable impurity, $\$$ H_2O , $*$ Grease, $\#$ Silicon grease).

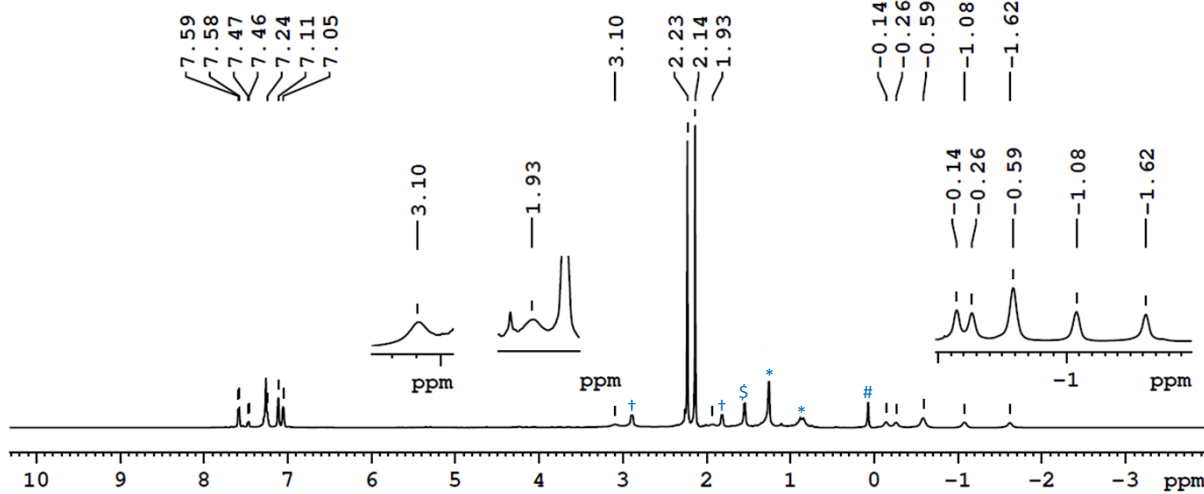


Figure S33. $^1\text{H}\{^{11}\text{B}\}$ NMR spectrum of **3b** in CDCl_3 (\ddagger Inseparable impurity, $\$$ H_2O , $*$ Grease, $\#$ Silicon grease).

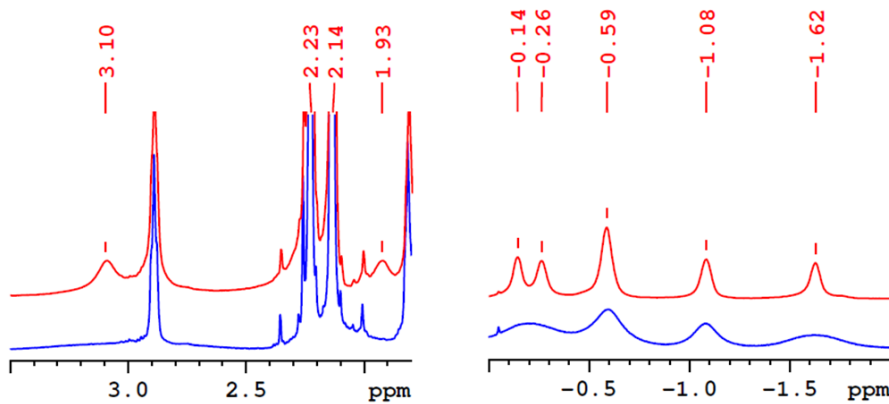


Figure S34. Stacked ^1H (bottom) and $^1\text{H}\{^{11}\text{B}\}$ NMR (top) spectra of **3b** in CDCl_3 .

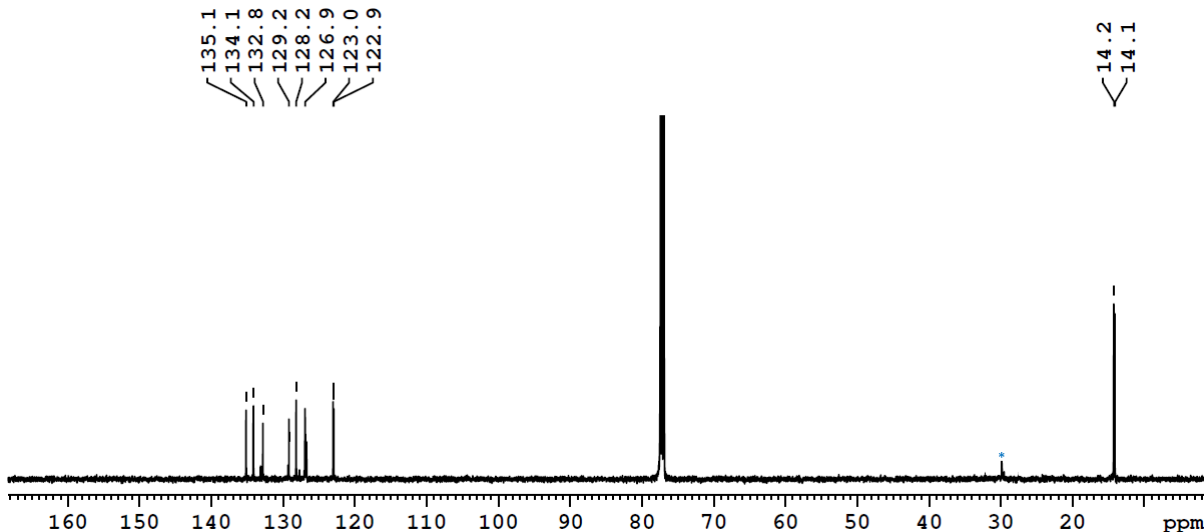


Figure S35. $^{13}\text{C}\{^1\text{H}\}$ NMR spectrum of **3b** in CDCl_3 (*Grease).

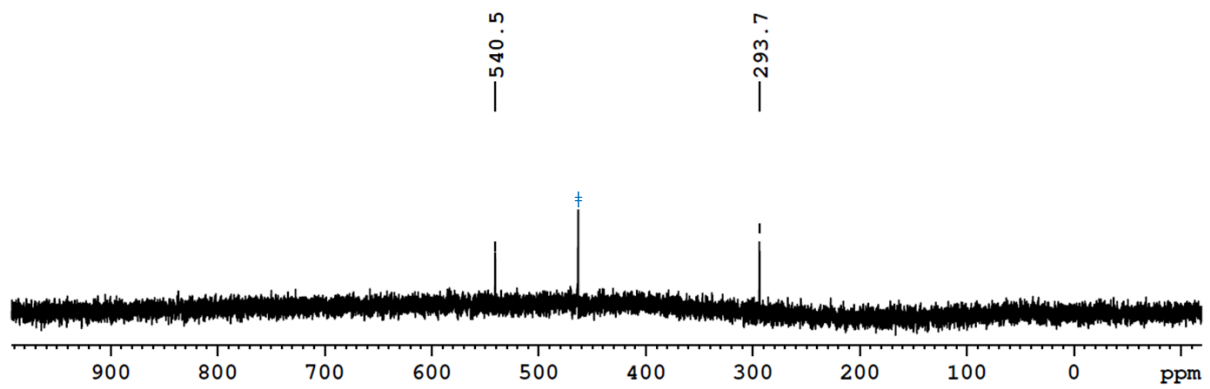


Figure S36. ^{77}Se NMR spectrum of **3b** in CDCl_3 (⊕ Peak at $\delta = 463$ ppm is due to the presence of Se_2Ph_2 as external reference).

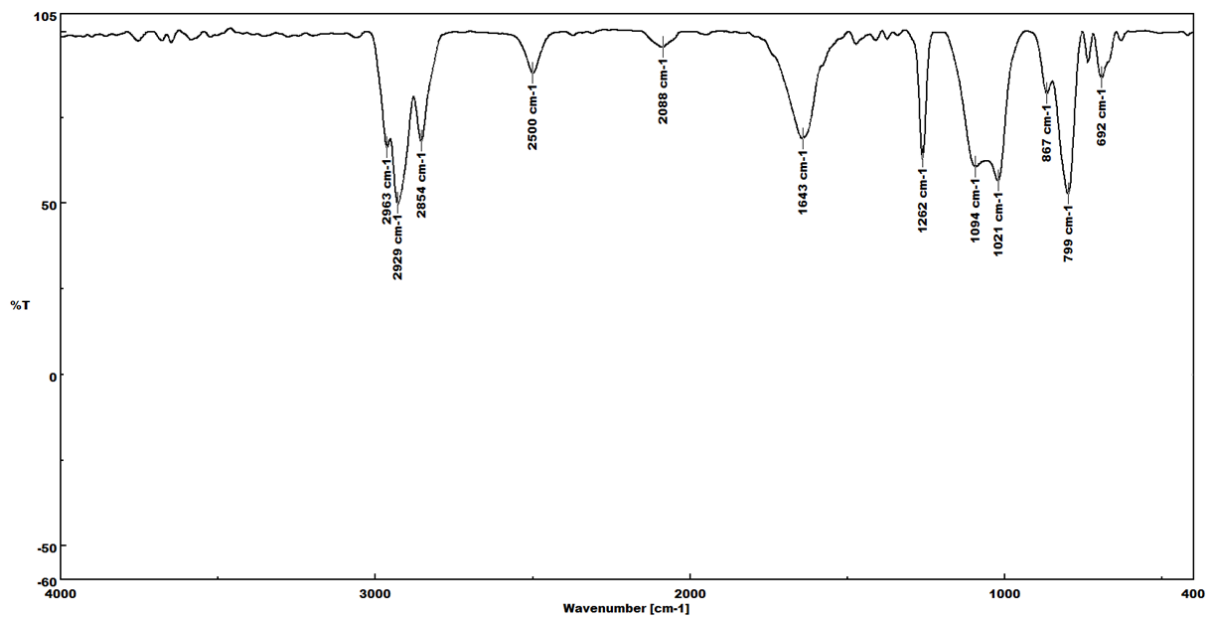


Figure S37. IR spectrum of **3b**.

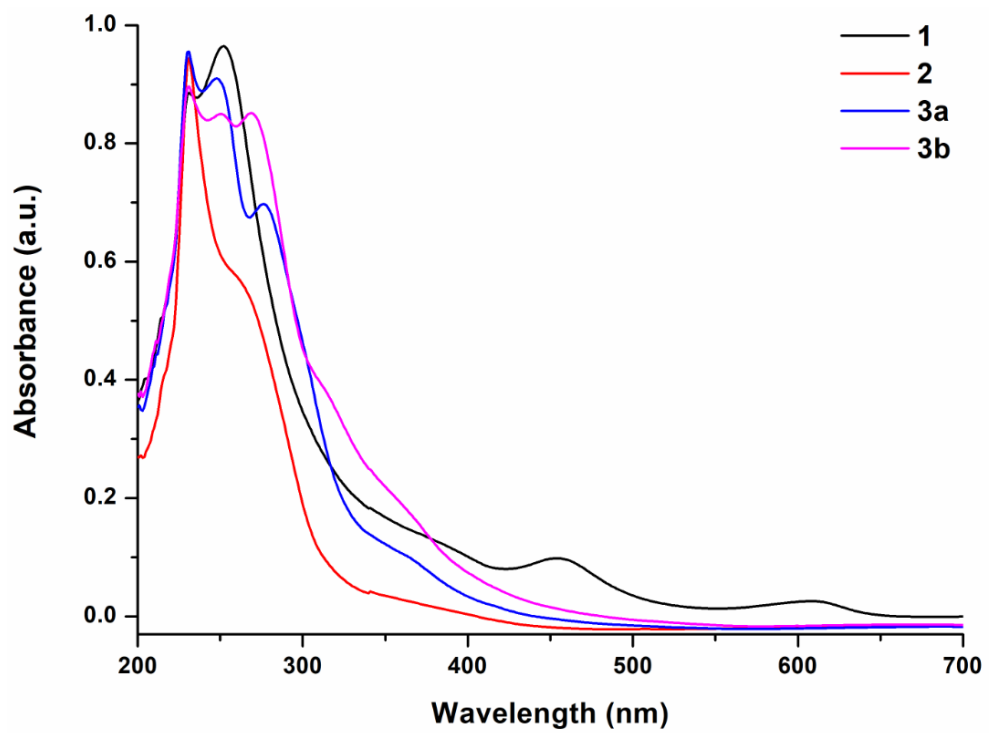


Figure S38. Combined UV-vis spectra of **1**, **2**, **3a**, and **3b** in CH_2Cl_2 .

I.4 X-ray Analysis Details

Suitable X-ray quality crystals of **1**, **2**, and **3b** were grown by slow diffusion of a hexane-dichloromethane (80:20 v/v) solution at 5 °C. Crystal data of **1** was obtained and integrated using a Bruker APEX3 SC-XRD with PHOTON II detector, with graphite monochromated MoK α ($\lambda = 0.71073$ Å) radiation at 302(2) K. Crystal data of **2** was obtained and integrated using a Bruker APEXII CCD diffractometer equipped with graphite monochromated MoK α ($\lambda = 0.71073$ Å) radiation at 296(2) K. And crystal data of **3b** was obtained and integrated using a Bruker Apex-III SC-XRD with PHOTON II detector, with graphite monochromated MoK α ($\lambda = 0.71073$ Å) radiation at 150(2) K. The structures were solved using SIR92^[10] and refined with SHELXT-2014/7.^[11] Using Olex2^[12], the molecular structures were drawn. Crystallographic data has been deposited with the Cambridge Crystallographic Data Center as supplementary publication no CCDC - 2353840 (**1**), 2321603 (**2**) and 2385700 (**3b**). The data can be obtained free of charge from The Cambridge Crystallographic Data Centre via www.ccdc.cam.ac.uk/data_request/cif.

Crystal data for **1**: $C_{30}H_{53}B_9Cl_2Ti_3$, $M_r = 725.52$, orthorhombic, space group $Pna2_1$, $a = 17.2436(17)$ Å, $b = 11.5096(10)$ Å, $c = 18.5384(16)$ Å, $\alpha = 90^\circ$, $\beta = 90^\circ$, $\gamma = 90^\circ$, $V = 3679.3(6)$ Å³, $Z = 4$, $\rho_{calcd} = 1.310$ g/cm³, $\mu = 0.802$ mm⁻¹, $F(000) = 1512$, $R_1 = 0.0594$, $wR_2 = 0.1413$, 3851 independent reflections [$2\theta \leq 41.67^\circ$] and 416 parameters.

Crystal data for **2**: $C_{30}H_{51}B_3Te_2Ti_3$, $M_r = 842.95$, triclinic, space group $P-1$, $a = 8.2544(3)$ Å, $b = 11.6397(5)$ Å, $c = 18.6492(8)$ Å, $\alpha = 91.086(3)^\circ$, $\beta = 91.102(2)^\circ$, $\gamma = 102.584(2)^\circ$, $V = 1747.93(12)$ Å³, $Z = 2$, $\rho_{calcd} = 1.602$ g/cm³, $\mu = 2.322$ mm⁻¹, $F(000) = 832$, $R_1 = 0.0632$, $wR_2 = 0.1660$, 6035 independent reflections [$2\theta \leq 50.76^\circ$] and 529 parameters.

Crystal data for **3b**: $C_{32}H_{49}B_5Se_2Ti_2$, $M_r = 741.42$, orthorhombic, space group $Pbca$, $a = 15.9297(12)$ Å, $b = 16.0271(12)$ Å, $c = 29.237(2)$ Å, $\alpha = 90^\circ$, $\beta = 90^\circ$, $\gamma = 90^\circ$, $V = 7464.4(9)$ Å³, $Z = 8$, $\rho_{calcd} = 1.319$ g/cm³, $\mu = 0.598$ mm⁻¹, $F(000) = 3024$, $R_1 = 0.0401$, $wR_2 = 0.0972$, 9346 independent reflections [$2\theta \leq 56.86^\circ$] and 407 parameters.

II Computational Details

All molecules were fully optimized using the *Gaussian 09*^[13] program employing the BP86 functional^[14] in conjunction with a def2-SVP basis set from the EMSL Basis Set Exchange Library.^[15] The model compounds were fully optimized in gaseous state (no solvent effect) starting from the X-ray crystallographic coordinates. Note that during optimization of **1**, Ti2...H1 distant was frozen and optimized. Note that the Ti-Ti bond becomes longer in clusters **1** and **2** in the optimized geometries as compared to the solid-state X-ray structures. Frequency calculations were performed at the same level of theory to verify the nature of the stationary states and the absence of any imaginary frequency to confirm that all structures represent minima on the potential energy hypersurface. Further, the gauge including atomic orbital (GIAO)^[16-18] method was employed to compute the ¹¹B chemical shifts. The NMR chemical shifts were calculated using the hybrid Becke–Lee–Yang–Parr (B3LYP) functional^[19] and the def2-SVP basis set on the BP86/def2-SVP optimized geometries. The ¹¹B NMR chemical shifts were calculated relative to B₂H₆ (B3LYP B shielding constant 84.05 ppm) and converted to the usual [BF₃.OEt₂] scale using the experimental δ (¹¹B) value of B₂H₆, 16.6 ppm.^[20] Natural bonding analyses were performed with the natural bond orbital (NBO) partitioning scheme^[21] as implemented in the Gaussian 09 suite of programs. Wiberg bond indexes (WBI)^[22] were obtained from a natural bond orbital analysis. In order to understand the nature of bonding in the synthesized molecules in greater detail, the topological properties of the resultant electron density, ρ , obtained from the wave functions of all the optimized structures were analyzed with the quantum theory of atoms in molecules (QTAIM).^[23] The QTAIM analysis was carried out utilizing the Multiwfns V.3.4 package^[24], whereas the wave functions were generated with Gaussian09 at the same level of theory as for geometry optimization. All the optimized structures and orbital graphics were generated using the Gaussview^[25], and Chemcraft^[26] visualization programs.

Table S1. Selected geometrical parameters^[a] and Wiberg bond indices (WBI) of **1**, **2**, **3a**, and **3b**.

1				2			
	Expt.	Cal.	WBI		Expt.	Cal.	WBI
Ti1-Ti2	3.292	3.537	0.286	Ti1-Ti2	2.57	3.049	0.630
T1-Ti3	3.073	3.142	0.421	T1-Ti3	3.09	3.316	0.382
Ti2-Ti3	3.026	3.025	0.535	Ti2-Ti3	2.947	3.267	0.438
Ti1-B1	2.513	2.450	0.361	Ti1-B1	2.52	2.41	0.335
Ti1-B7	2.347	2.283	0.433	Ti1-B2	2.266	2.366	0.406
Ti1-B9	2.494	2.245	0.693	Ti1-Te1	2.558	2.730	0.843
Ti2-B7	2.386	2.359	0.402	Ti2-B1	2.57	2.358	0.402
Ti3-B4	2.529	2.597	0.369	Ti2-B2	2.289	2.232	0.461
B7-B8	1.66	1.662	0.686	Ti2-B3	2.485	2.422	0.330
B5-B6	1.74	1.755	0.559	Ti2-Te2	2.658	2.791	0.763
B8-H1	1.19	1.188	0.594	Ti3-B2	2.279	2.299	0.496
Ti2-H1	1.95	1.945	0.204	Ti3-Te1	2.630	2.733	0.983
B7-Cl1	1.854	1.987	1.643	B1-B2	1.57	1.753	0.753
Ti1-Cl1	2.543	2.686	0.437	B2-B3	1.718	1.739	0.772
Ti2-Cl2	2.407	2.468	0.616	B2-Te1	2.341	2.272	0.815
3a				3b			
	Expt.	Cal.	WBI		Expt.	Cal.	WBI
Ti1-Ti2	-	3.049	0.344	Ti1-Ti2	3.028	3.056	0.332
Ti1-B1	-	2.568	0.250	Ti1-B1	2.545	2.542	0.260
Ti1-B3	-	2.270	0.533	Ti1-B3	2.271	2.284	0.530
Ti1-B4	-	2.551	0.255	Ti1-B4	2.554	2.548	0.256
Ti2-B2	-	2.546	0.260	Ti2-B2	2.612	2.645	0.223
Ti2-B3	-	2.254	0.544	Ti2-B3	2.254	2.258	0.541
Ti2-B5	-	2.549	0.263	Ti2-B5	2.542	2.532	0.267
Ti1-Se1	-	2.667	0.760	Ti1-Se1	2.645	2.655	0.768
Ti1-Se2	-	2.485	1.173	Ti1-Se2	2.459	2.486	1.169
B1-B2	-	1.782	0.558	B1-B2	1.784	1.790	0.552
B1-B3	-	1.714	0.643	B1-B3	1.700	1.713	0.636
B2-B3	-	1.711	0.647	B2-B3	1.717	1.731	0.636
B4-B5	-	1.788	0.5518	B4-B5	1.787	1.789	0.548
				B2-C1	1.587	1.599	0.887
				Se1-C2	1.953	1.976	0.97

^[a] Note that the Ti-Ti bond becomes longer in clusters **1** and **2** in the optimized geometries as compared to the solid-state X-ray structures.

Table S2. Selected experimental and Calculated bond angles of **1**, **2**, **3a**, and **3b**.

1			2		
	Expt.	Cal.		Expt.	Cal.
Ti1-Ti2-Ti3	58.01	56.56	Ti1-Ti2-Ti3	60.30	63.21
Ti2-Ti3-Ti1	63.34	69.97	Ti2-Ti3-Ti1	63.79	55.18
Ti3-Ti2-Ti2	56.65	53.46	Ti3-Ti2-Ti2	55.90	61.60
Ti1-B9-Ti3	91.3	89.27	Ti1-B2-Ti2	89.0	83.03
Ti1-Cl2-Ti3	78.01	76.72	Ti-B2-Ti3	85.7	90.57
Ti1-Cl1-B1	62.2	56.10	Ti2-B2-Ti3	80.3	92.27
Ti2-H1-Ti3	94.50	94.51	Ti-B1-Ti2	77.54	79.49
Ti2-H1-B8	89.35	84.79	Ti1-Te2-Ti2	77.78	66.67
Ti3-B3-B6	119.2	117.89	Ti1-Te1-Ti3	77.13	74.75
B3-B6-B5	113.7	112.21	Ti-B1-B2	62.25	62.11
			B1-B2-B3	112.5	119.64
3a			3b		
	Expt.	Cal.		Expt.	Cal.
Ti1-B3-Ti2	-	84.74	Ti1-B3-Ti2	84.03	84.56
Ti1-B1-B2	-	104.13	Ti1-B1-B2	105.6	106.79
Ti1-Ti2-B2	-	75.93	Ti1-Ti2-B2	75.76	75.81
B1-B3-B2	-	62.69	B1-B3-B2	62.96	62.59
B1-B3-B5	-	156.01	B1-B3-B5	155.9	158.09
Ti-Se1Ti2	-	69.14	Ti-Se1Ti2	69.51	69.35
Ti1-Se2-Ti2	-	75.86	Ti1-Se2-Ti2	75.97	75.08

Table S3. Calculated natural charges (q) and natural valence population (Pop) of **1**, **2**, **3a**, and **3b**.

1			2		
	q	Pop(val)		q	Pop(val)
Ti1	0.523	3.246	Ti1	0.099	3.909
Ti2	0.085	3.816	Ti2	0.159	3.855
Ti3	0.392	3.452	Ti3	0.0878	3.924
B1	-0.366	3.330	B1	-0.356	3.337
B2	-0.276	3.237	B2	-0.289	3.248
B3	-0.219	3.185	B3	-0.363	3.344
B4	-0.258	3.226	Te1	0.298	5.698
B5	-0.178	3.143	Te2	0.057	5.939
B6	-0.233	3.198			
B7	-0.027	2.993			

B8	-0.161	3.123			
B9	-0.301	3.264			
Cl1	0.189	6.788			
Cl2	0.136	6.834			
3a			3b		
	q	Pop(val)		q	Pop(val)
Ti1	0.048	3.961	Ti1	0.103	3.976
Ti2	0.056	3.954	Ti2	0.033	3.908
B1	-0.184	3.168	B1	-0.190	3.173
B2	-0.184	3.169	B2	0.081	2.894
B3	-0.340	3.300	B3	-0.344	3.307
B4	-0.175	3.159	B4	-0.176	3.160
B5	-0.178	3.162	B5	-0.186	3.171
Se1	0.216	5.762	Se1	0.219	5.760
Se2	-0.020	6.015	Se2	-0.021	6.015

Table S4. Calculated HOMO–LUMO energy gap of **1**, **2**, **3a**, and **3b**.

	1	2	3a	3b
$\Delta E_{\text{H-L}}$ (eV)	1.63	1.70	1.773	1.783

Table S5. Calculated chemical shifts for complexes **1**, **2**, **3a**, and **3b**.

Compounds	¹¹ B NMR value (ppm)	
	Experimental	Theoretical
1	31.6	11.1, 13.4, 16.6, 18.45
	40.0	35.9, 37.2
	45.0	52.4
	52.3	67.5
	66.4	84.5
2	-7.7	-10.4, 6.9
	54.0	62.7
3a	-2.2	-10.2, -9.1
	0.8	-7.0, -4.5
	51.3	37.3
3b	-0.3	-8.9
	1.4	-5.9, -4.6
	5.2	-0.5
	50.6	35.8

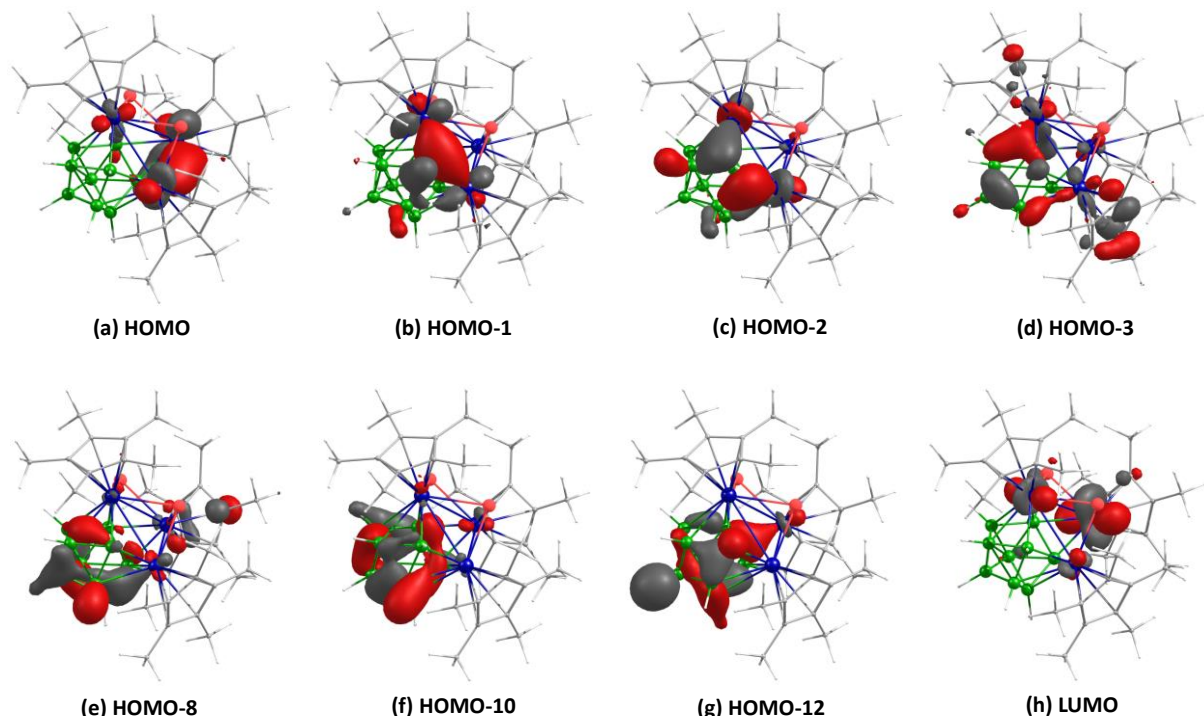


Figure S39. Selected molecular orbitals of **1** (isocontour values: ± 0.045 [e.bohr $^{-3}$] $^{1/2}$).

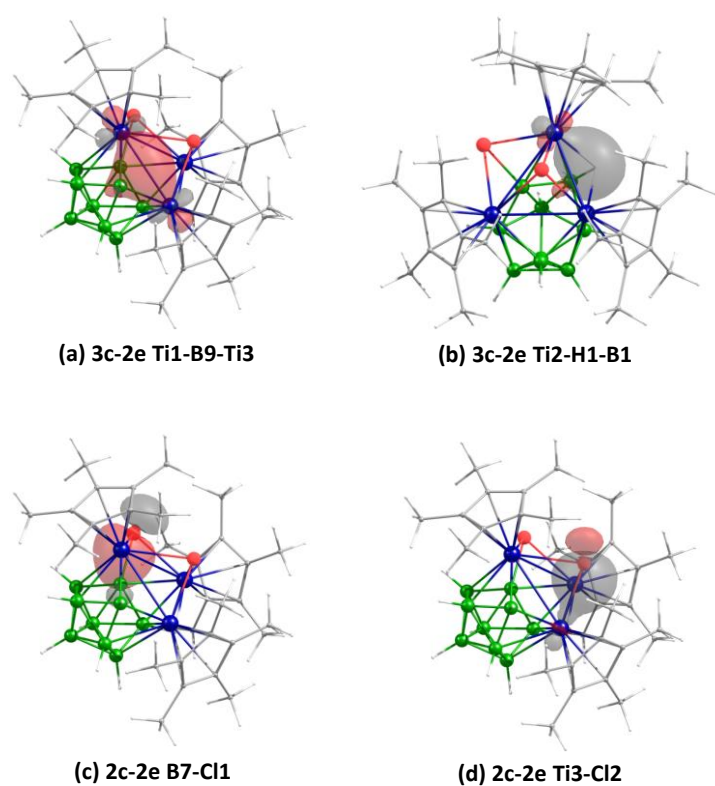


Figure S40. Selected NBO interactions of **1** (isocontour values: ± 0.045 [e.bohr $^{-3}$] $^{1/2}$).

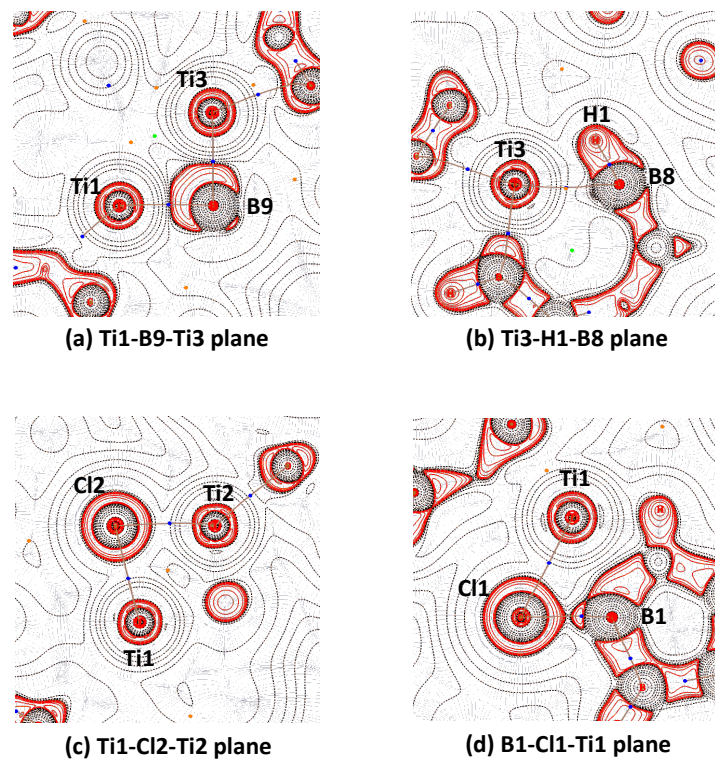


Figure S41. Contour-line diagram of the Laplacian of the electron density of **1** in selected planes. The solid brown lines are bond paths, whereas blue dots indicate the bond-critical points (BCP). Solid red lines indicate the areas of charge concentration ($\nabla^2\rho(r) < 0$), while dashed black lines show the areas of charge depletion ($\nabla^2\rho(r) > 0$).

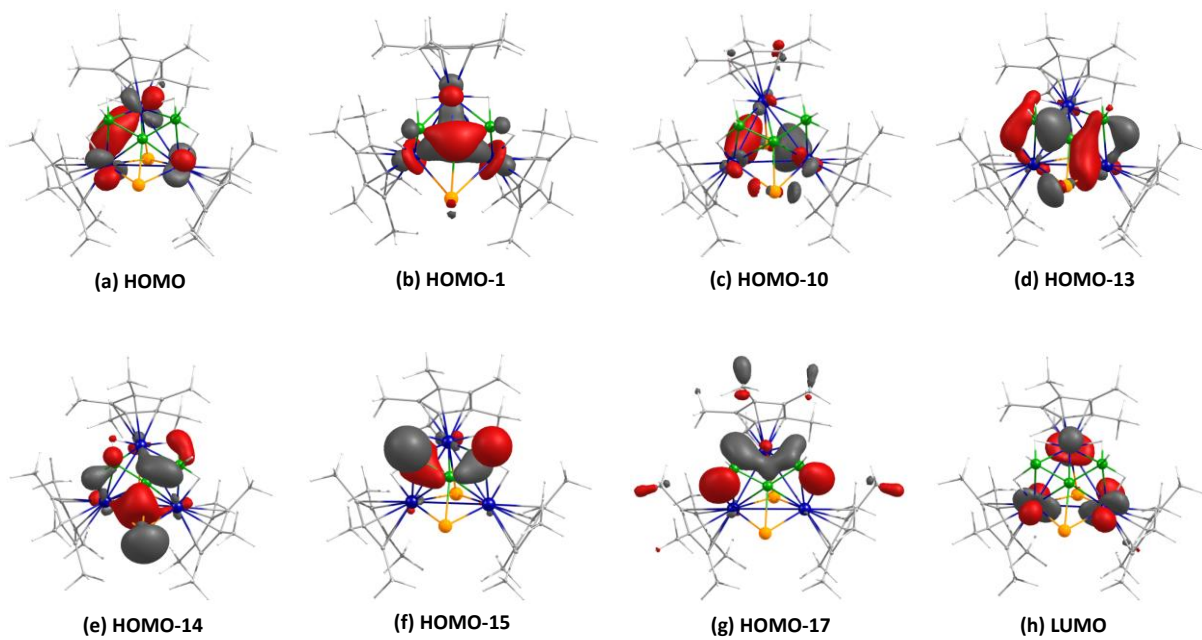


Figure S42. Selected molecular orbitals of **2** (isocontour values: $\pm 0.045 \text{ [e.bohr}^{-3}]^{1/2}$).

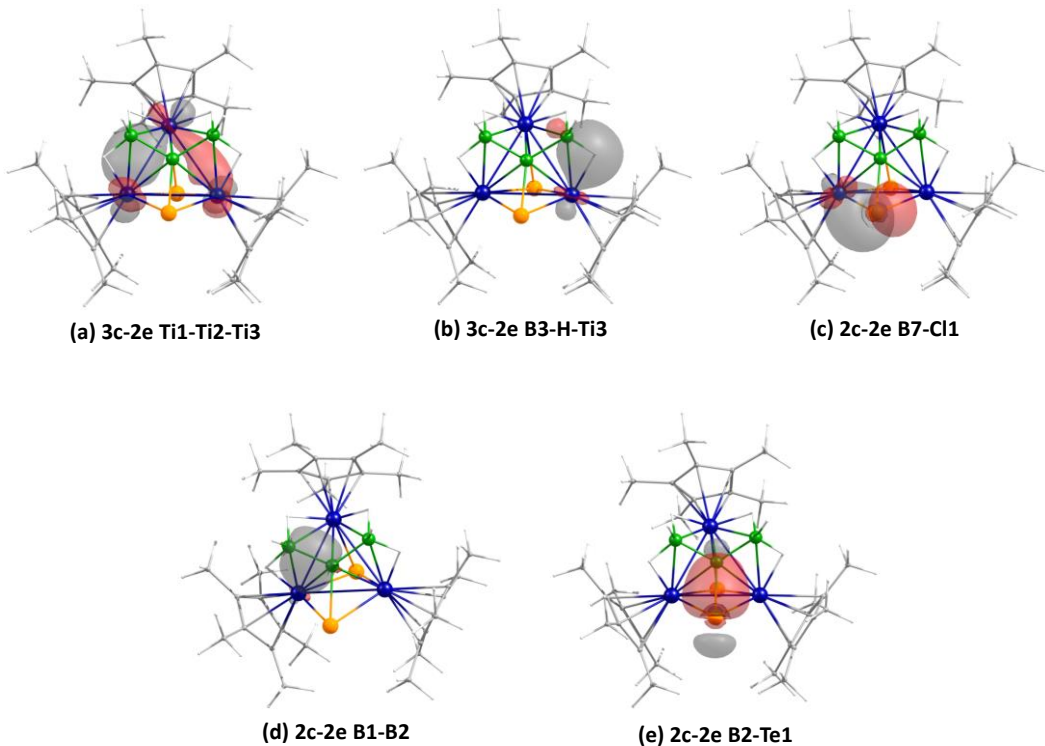


Figure S43. Selected NBO interactions of **2** (isocontour values: $\pm 0.045 \text{ [e.bohr}^{-3}]^{1/2}$).

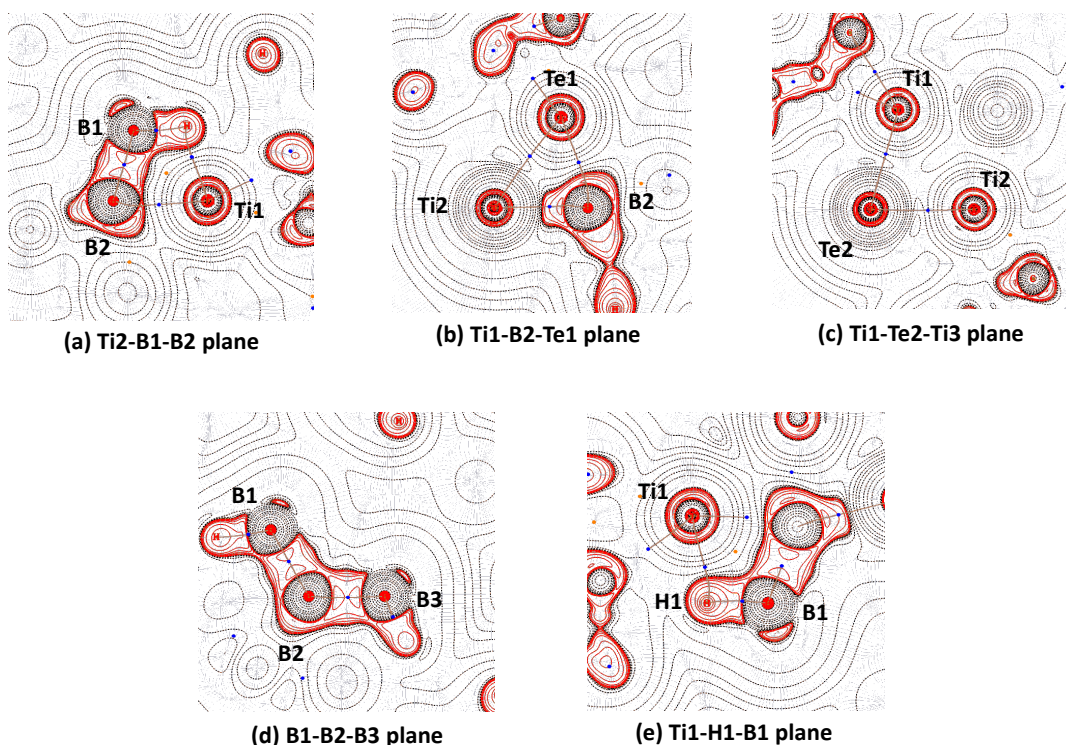


Figure S44. Contour-line diagram of the Laplacian of the electron density of **2** in selected planes. The solid brown lines are bond paths, whereas blue dots indicate the bond-critical points (BCP). Solid red lines indicate the areas of charge concentration ($\nabla^2 \rho(r) < 0$), while dashed black lines show the areas of charge depletion ($\nabla^2 \rho(r) > 0$).

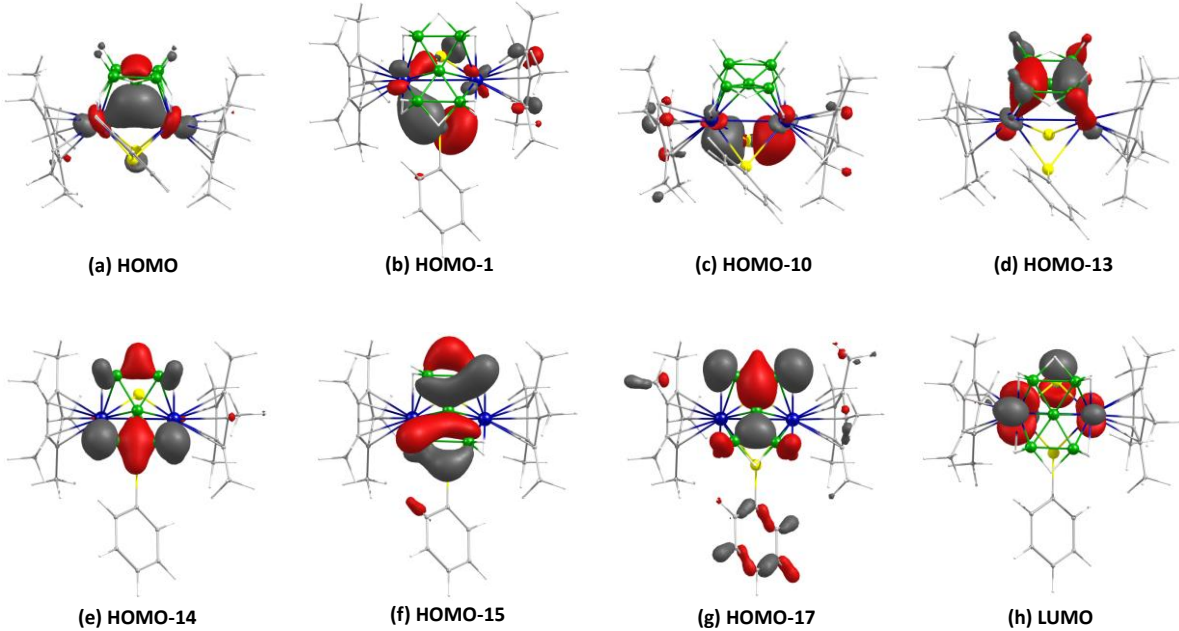


Figure S45. Selected molecular orbitals of **3a** (isocontour values: ± 0.045 [e.bohr $^{-3}^{1/2}$]). A comparison of the MO energies of **3a** (1.77 eV) and **3b** (1.78 eV) reveals comparable HOMO-LUMO gaps. Given the structural and bonding similarities between clusters **3a** and **3b**, this analysis focuses on the detailed bonding characteristics of cluster **3a**. The HOMO of **3a** exhibits overlap of d orbitals between the two titanium centers and d-p interactions between the titanium centers and the boride boron atom (B3), indicating strong bonding interactions between the titanium centers and significant metal-boride interactions (Fig. S45a). The WBI of 0.34 for the Ti1-Ti2 bond (Table S1) further corroborates the presence of metal-metal interaction. The LUMO of **3a** is primarily localized on the Ti1, Ti2, and Se2 centers (Figure S45h). HOMO-1 and HOMO-14 demonstrate d-p orbital interactions of Ti-S bonds (Figure S45b-c), which are also evident in the contour line map in the Ti1-Se1-Ti2 plane (Figure 47f). Additionally, HOMO-13, HOMO-14, HOMO-15, and HOMO-17 of **3a** illustrate metal-boron and boron-boron bonding interactions (Figure S45d-g).

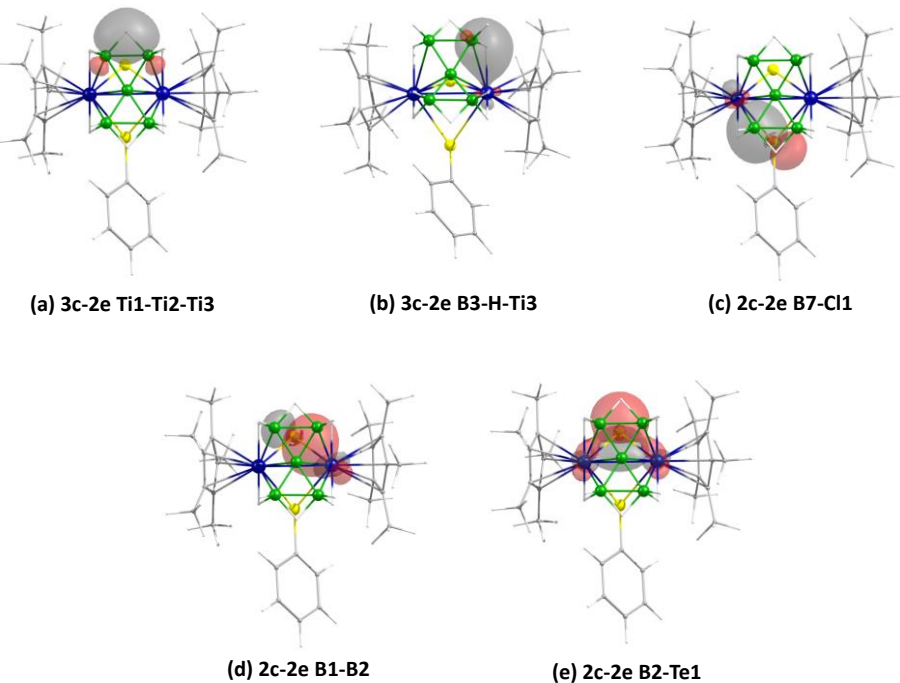


Figure S46. Selected NBO interactions of **3a** (isocontour values: ± 0.045 [e.bohr $^{-3}^{1/2}$]). The NBO analysis of compound **3a** corroborates the MO findings previously discussed. NBO analysis provides a localized description of electronic structure, offering complementary insights to the MO analysis.

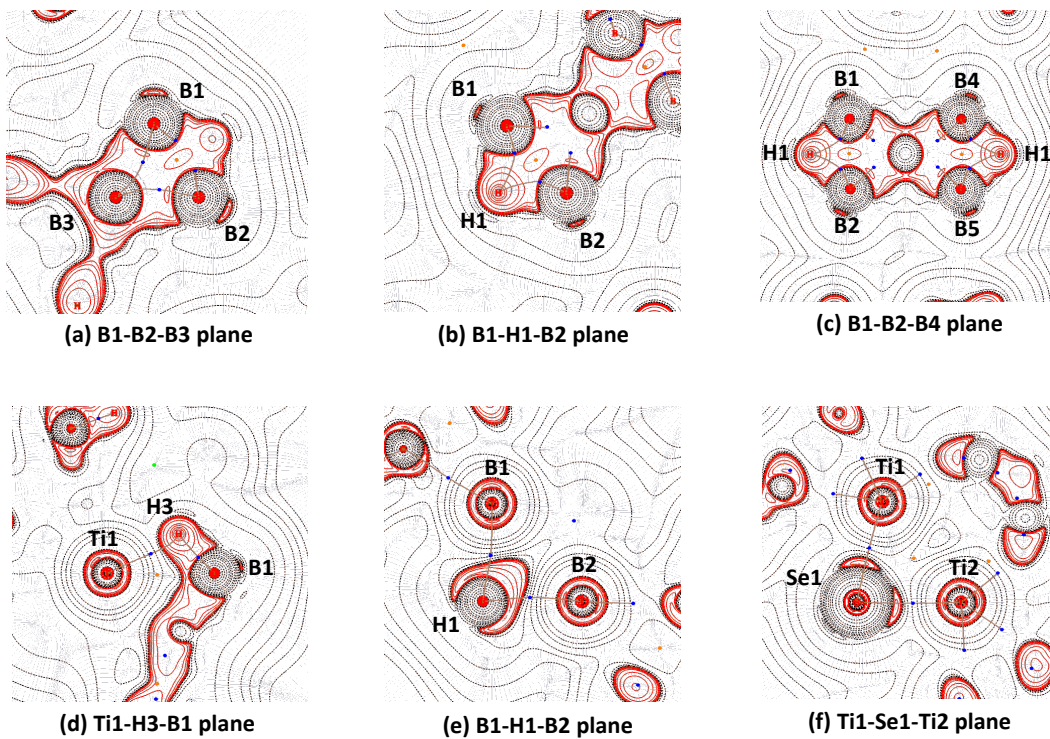


Figure S47. Contour-line diagram of the Laplacian of the electron density of **3a** in selected planes. The solid brown lines are bond paths, whereas blue dots indicate the bond-critical points (BCP). Solid red lines indicate the areas of charge concentration ($\nabla^2\rho(r) < 0$), while dashed black lines show the areas of charge depletion ($\nabla^2\rho(r) > 0$). The contour line plot along the B1-B2-B3 plane shows a high amount of charge concentrations and the BCPs between B1-B3 and B2-B3 bonds specified strong bonding interactions of the boride boron with the peripheral boron atoms (Figure S47a). This is also supported by the WBI of those particular bonds. Furthermore, the Laplacian electron density plot of **3a** shows the bonding scenario of the pentaborane plane, which is coordinated symmetrically to both metal centers (Fig. S47c).

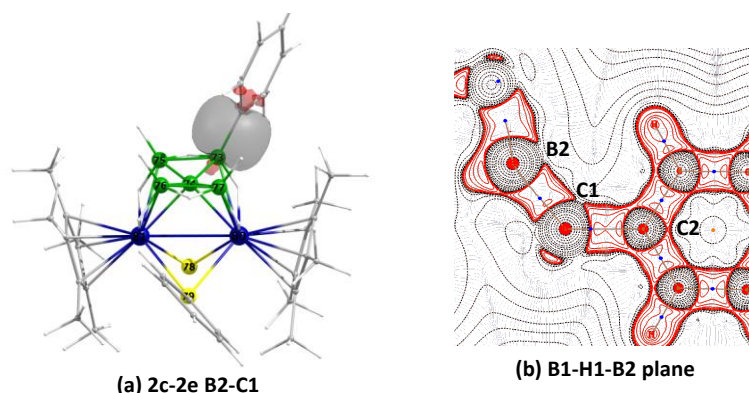


Figure S48. (a) Selected NBO interaction of **3b** (isocontour values: $\pm 0.045 \text{ [e.bohr}^{-3}]^{1/2}$). (b) Contour-line diagram of the Laplacian of the electron density of **3b** along B2-C1-C2 plane. The solid brown lines are bond paths, whereas blue dots indicate the bond-critical points (BCP). Solid red lines indicate the areas of charge concentration ($\nabla^2\rho(r) < 0$), while dashed black lines show the areas of charge depletion ($\nabla^2\rho(r) > 0$). The NBO analysis depicts the 2c-2e B2-C1 interaction of $\text{B}_5\text{H}_9\text{Ph}$ fragment in **3b**, which is also reflected in the contour line map in the B2-C1-C2 plane.

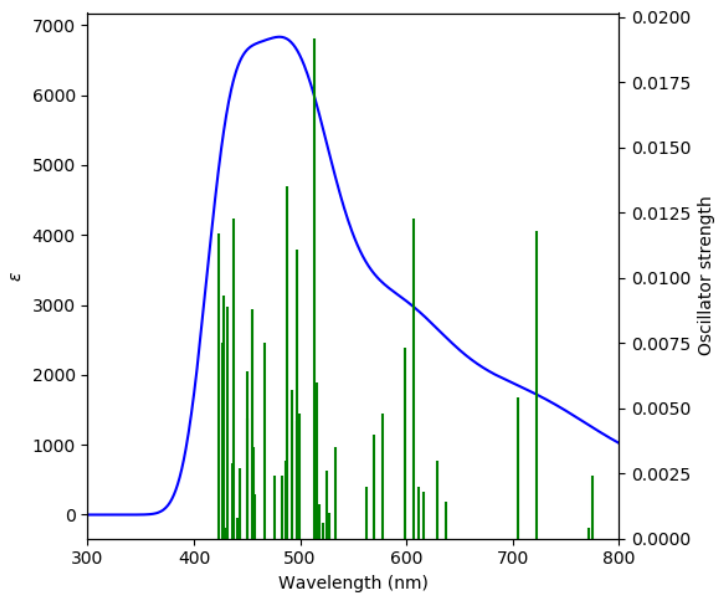


Figure S49. Absorption spectrum of **1** computed at TD-DFT-B3LYP/Def2-SVP level of theory (ε in $\text{LM}^{-1}\text{cm}^{-1}$).

Table S6. TD-DFT calculated energies (excitation energy (eV), λ_{calc} (nm)), oscillator strength (f), and main composition of the first UV-vis electronic excitations for **1**. Experimental absorption wavelengths (λ_{exp} , nm) of **1** are given for comparison.

No	Excitation Energy (eV)	Wavelength λ (nm)		Main electronic transition (% weight) ^[b]
		Calc. (f) ^[a]	Expt.	
1	1.716	722 (0.012)		HOMO→LUMO+4 (77)
2	2.044	606 (0.012)	607	HOMO-2→LUMO+2 (32) HOMO→LUMO+5 (29) HOMO-4→LUMO (13)
3	2.417	513 (0.019)		HOMO-4→LUMO+2 (37) HOMO-3→LUMO+2 (26)
4	2.493	497 (0.011)		HOMO-8→LUMO (54) HOMO-6→LUMO+1 (13)
5	2.542	488 (0.013)	455	HOMO-6→LUMO+1 (25) HOMO-6→LUMO+2 (25) HOMO-2→LUMO+4 (20)
6	2.837	437 (0.012)		HOMO→LUMO+9 (23) HOMO-5→LUMO+3 (21) HOMO-1→LUMO+6 (17) HOMO-9→LUMO+1 (11)
7	2.925	424 (0.012)		HOMO-4→LUMO+4 (50) HOMO-3→LUMO+4 (19)

^[a]Oscillator strength greater than 0.010 and ^[b]Components with greater than 10% contribution shown.

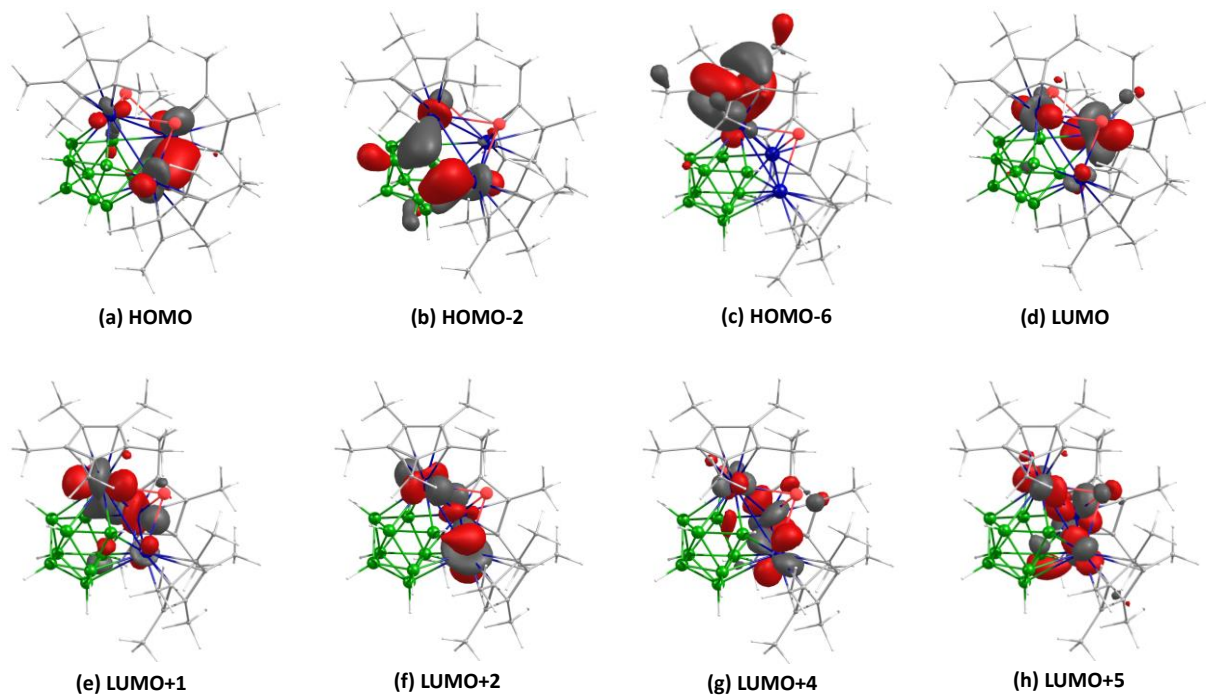


Figure S50. Selected molecular orbitals of **1** related to most intense electronic transitions [isocontour values: ± 0.045 ($e/\text{bohr}^3)^{1/2}$].

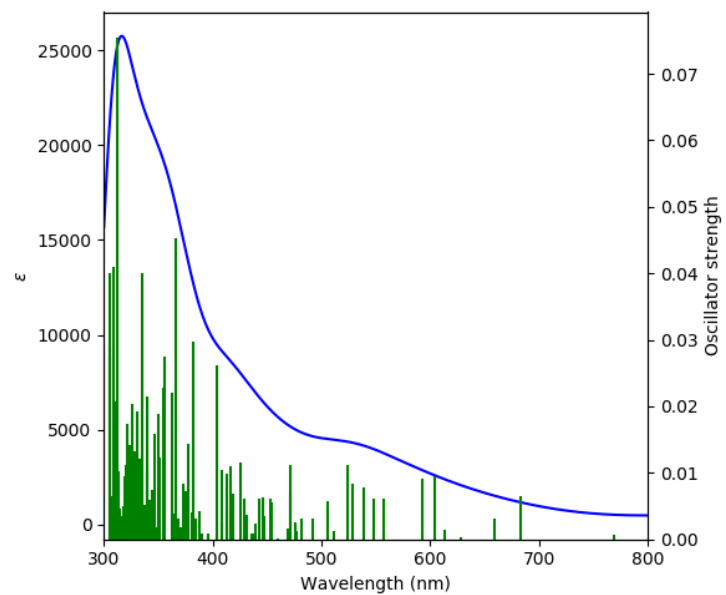


Figure S51. Absorption spectrum of **2** computed at TD-DFT-B3LYP/Def2-SVP level of theory (ϵ in $\text{LM}^{-1}\text{cm}^{-1}$).

Table S7. TD-DFT calculated energies (excitation energy (eV), λ_{calc} (nm)), oscillator strength (f), and main composition of the first UV-vis electronic excitations for **2**. Experimental absorption wavelengths (λ_{exp} , nm) of **2** are given for comparison.

No	Excitation Energy (eV)	Wavelength λ (nm)		Main electronic transition (% weight) ^[b]
		Calc. (f) ^[a]	Expt.	
1	3.068	404 (0.026)		HOMO-7→LUMO+2 (22)
				HOMO-9→LUMO+1 (16)
2	3.246	382 (0.030)		HOMO-12→LUMO (25)
				HOMO-1→LUMO+7 (19)
3	3.391	366 (0.045)		HOMO-6→LUMO+3 (27)
				HOMO-10→LUMO+2 (18)
				HOMO-1→LUMO+8 (15)
4	3.416	363 (0.022)		HOMO-1→LUMO+9 (55)
				HOMO-3→LUMO+4 (19)
5	3.482	356 (0.027)		HOMO-2→LUMO+5 (25)
				HOMO-3→LUMO+4 (18)
6	3.542	350 (0.019)		HOMO-11→LUMO+2 (35)
				HOMO-8→LUMO+3 (13)
				HOMO-2→LUMO+5 (12)
				HOMO-1→LUMO+10 (12)
7	3.577	347 (0.016)		HOMO-2→LUMO+6 (81)
8	3.647	340 (0.022)		HOMO-12→LUMO+1 (25)
				HOMO-1→LUMO+10 (14)
				HOMO-9→LUMO+3 (11)
				HOMO-1→LUMO+11 (14)
9	3.697	335 (0.040)	346	HOMO-3→LUMO+6 (20)
				HOMO-3→LUMO+5 (11)
10	3.748	331 (0.019)		HOMO-6→LUMO+4 (25)
				HOMO→LUMO+14 (23)
				HOMO-10→LUMO+3 (19)

^[a]Oscillator strength greater than 0.010 and ^[b]Components with greater than 10% contribution shown.

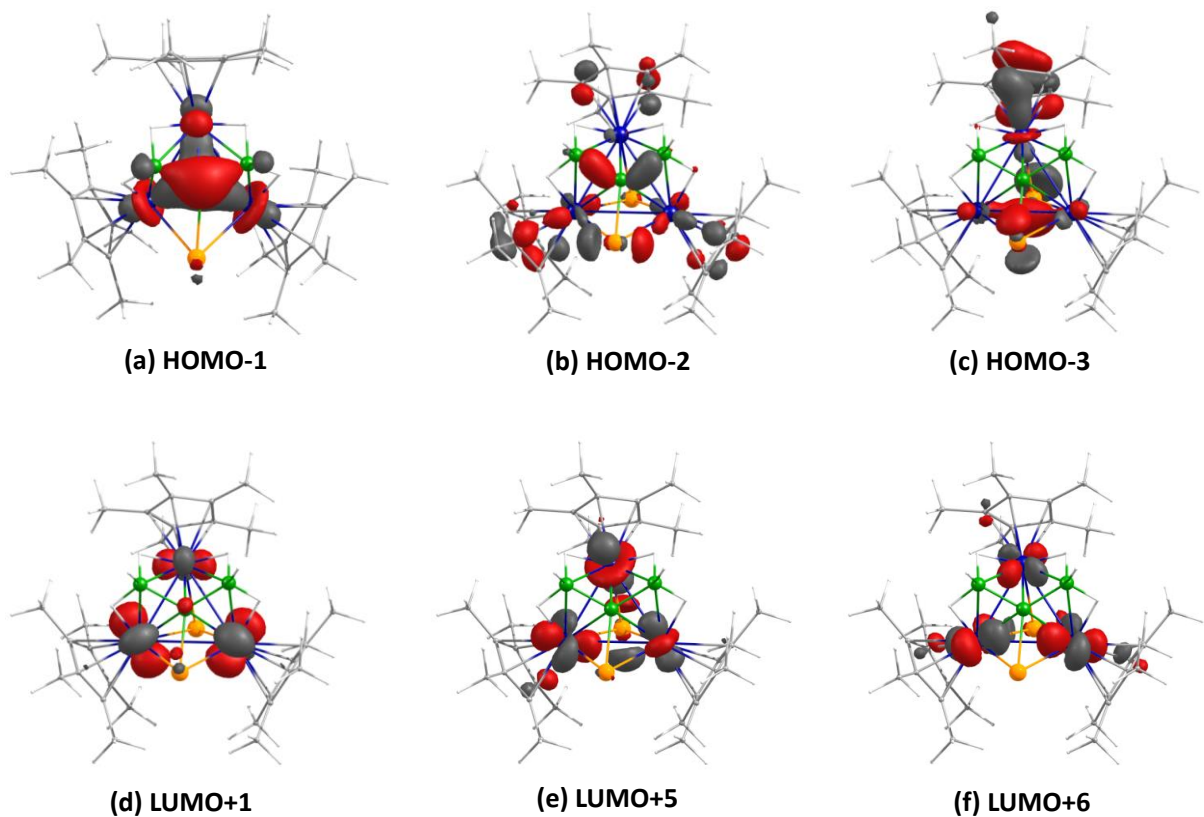


Figure S52. Selected molecular orbitals of **2** related to most intense electronic transitions [isocontour values: ± 0.045 ($e/\text{bohr}^3\right)^{1/2}$].

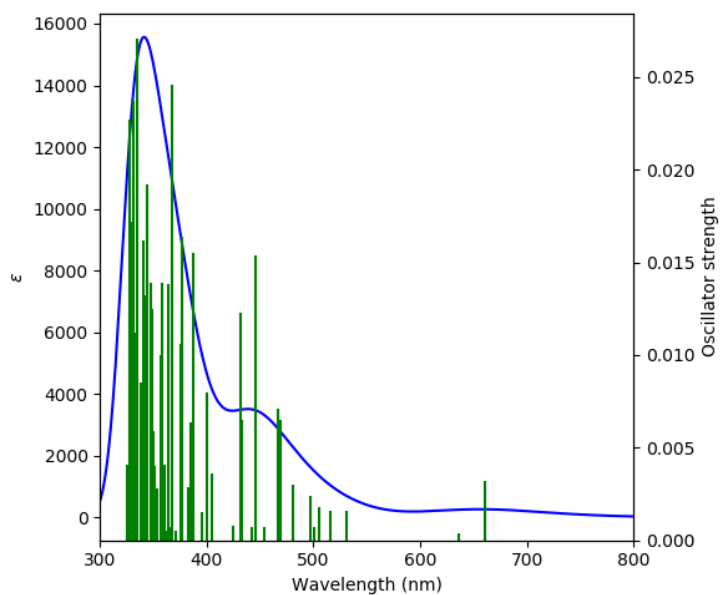


Figure S53. Absorption spectrum of **3a** computed at TD-DFT-B3LYP/Def2-SVP level of theory (ϵ in $\text{LM}^{-1}\text{cm}^{-1}$).

Table S8. TD-DFT calculated energies (excitation energy (eV), λ_{calc} (nm)), oscillator strength (f), and main composition of the first UV-vis electronic excitations for **3a**. Experimental absorption wavelengths (λ_{exp} , nm) of **3a** are given for comparison.

No	Excitation Energy (eV)	Wavelength λ (nm)		Main electronic transition (% weight) ^[b]
		Calc. (f) ^[a]	Expt.	
1	2.784	445 (0.015)		HOMO \rightarrow LUMO+2 (84)
2	2.874	431 (0.012)		HOMO-6 \rightarrow LUMO+1 (60)
				HOMO-6 \rightarrow LUMO (14)
3	3.203	387 (0.016)		HOMO \rightarrow LUMO+5 (49)
				HOMO \rightarrow LUMO+6 (15)
4	3.293	377 (0.016)		HOMO-2 \rightarrow LUMO+2 (64)
				HOMO-8 \rightarrow LUMO+1 (12)
5	3.305	375 (0.011)		HOMO-8 \rightarrow LUMO+1 (74)
				HOMO-2 \rightarrow LUMO+2 (12)
6	3.379	367 (0.025)	364	HOMO-3 \rightarrow LUMO+2 (63)
				HOMO-1 \rightarrow LUMO+3 (21)
7	3.411	363 (0.014)		HOMO-4 \rightarrow LUMO+2 (59)
				HOMO \rightarrow LUMO+6 (21)
8	3.461	358 (0.014)		HOMO \rightarrow LUMO+6 (18)
				HOMO-4 \rightarrow LUMO+2 (17)
				HOMO-10 \rightarrow LUMO+1 (15)
				HOMO-5 \rightarrow LUMO+2 (12)
9	3.558	348 (0.013)		HOMO-3 \rightarrow LUMO+3 (64)
10	3.571	347 (0.014)		HOMO \rightarrow LUMO+7 (24)
				HOMO-5 \rightarrow LUMO+2 (18)
				HOMO-11 \rightarrow LUMO (17)

^[a]Oscillator strength greater than 0.010 and ^[b]Components with greater than 10% contribution shown.

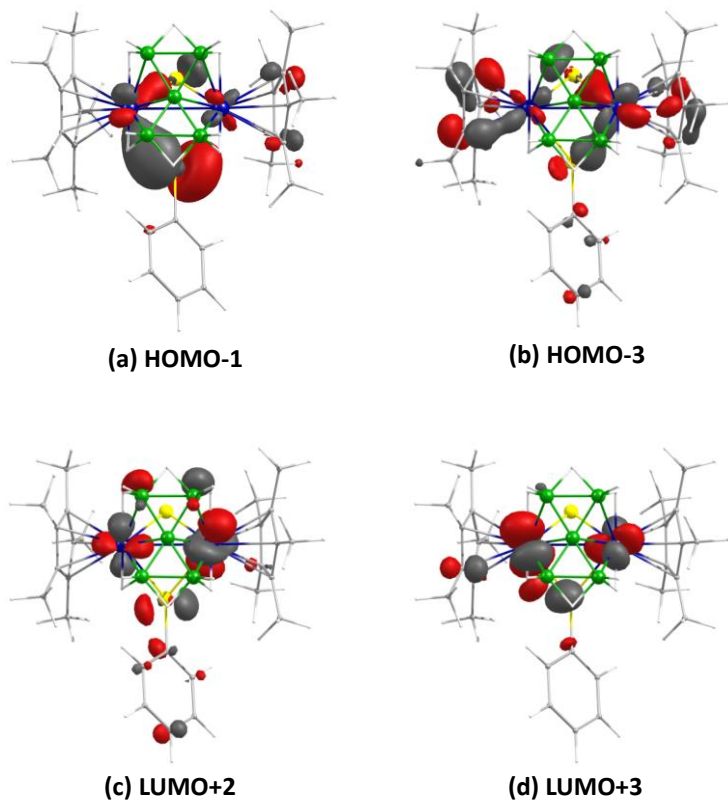


Figure S54. Selected molecular orbitals of **3a** related to most intense electronic transitions [isocontour values: ± 0.045 ($e/\text{bohr}^3\right)^{1/2}$].

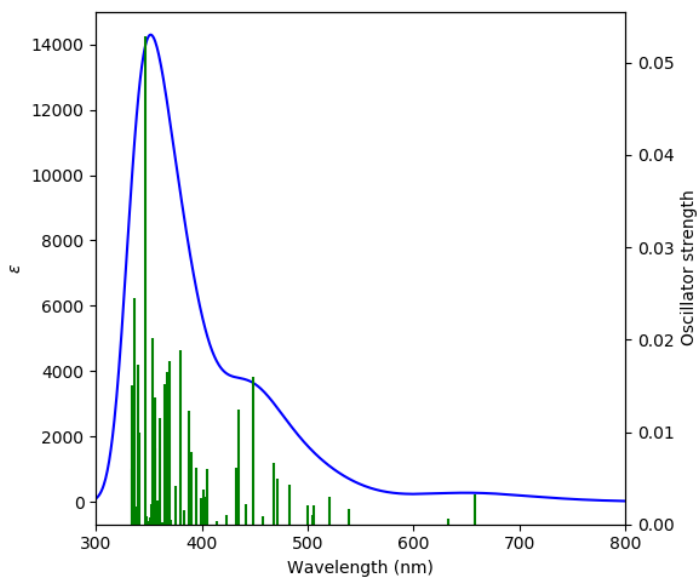


Figure S55. Absorption spectrum of **3b** computed at TD-DFT-B3LYP/Def2-SVP level of theory (ε in $\text{LM}^{-1}\text{cm}^{-1}$).

Table S9. TD-DFT calculated energies (excitation energy (eV), λ_{calc} (nm)), oscillator strength (f), and main composition of the first UV-vis electronic excitations for **3b**. Experimental absorption wavelengths (λ_{exp} , nm) of **3b** are given for comparison.

No	Excitation Energy (eV)	Wavelength λ (nm)		Main electronic transition (% weight) ^[b]
		Calc. (f) ^[a]	Expt.	
1	2.767	448 (0.016)		HOMO \rightarrow LUMO+2 (85)
2	2.849	435 (0.012)		HOMO-4 \rightarrow LUMO (21)
				HOMO-2 \rightarrow LUMO (16)
				HOMO-6 \rightarrow LUMO (13)
3	3.200	387 (0.012)		HOMO \rightarrow LUMO+5 (38)
				HOMO-10 \rightarrow LUMO (11)
4	3.259	380 (0.019)		HOMO-2 \rightarrow LUMO+2 (74)
5	3.352	370 (0.018)		HOMO-3 \rightarrow LUMO+2 (73)
6	3.374	367 (0.017)		HOMO-1 \rightarrow LUMO+3 (80)
7	3.398	365 (0.015)	366	HOMO-4 \rightarrow LUMO+2 (61)
				HOMO \rightarrow LUMO+6 (22)
8	3.440	360 (0.012)		HOMO-1 \rightarrow LUMO+4 (28)
				HOMO-4 \rightarrow LUMO+2 (14)
				HOMO-5 \rightarrow LUMO+2 (14)
				HOMO \rightarrow LUMO+6 (13)
9	3.487	356 (0.014)		HOMO \rightarrow LUMO+7 (54)
				HOMO-1 \rightarrow LUMO+4 (15)
10	3.509	353 (0.020)		HOMO-5 \rightarrow LUMO+2 (39)
				HOMO \rightarrow LUMO+6 (11)

^[a]Oscillator strength greater than 0.010 and ^[b]Components with greater than 10% contribution shown.

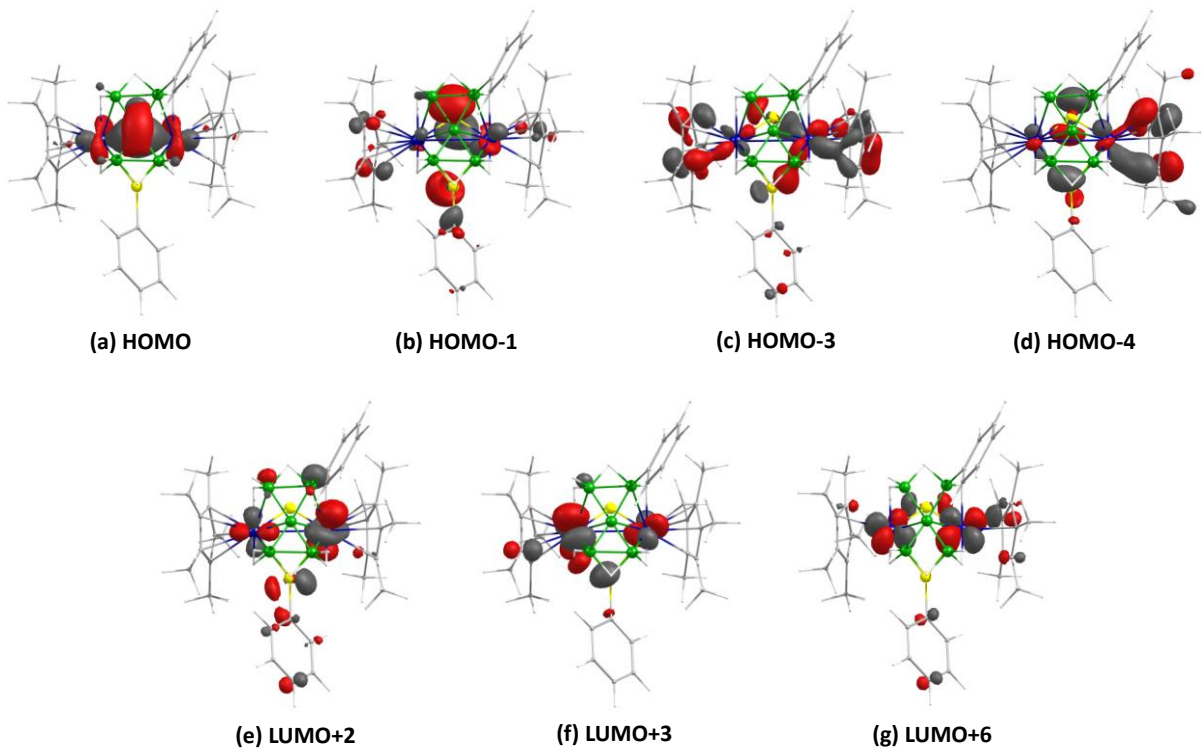


Figure S56. Selected molecular orbitals of **3b** related to most intense electronic transitions [isocontour values: ± 0.045 ($e/\text{bohr}^{3/2}$) $^{1/2}$].

III Cartesian Coordinates of all Optimized Structures

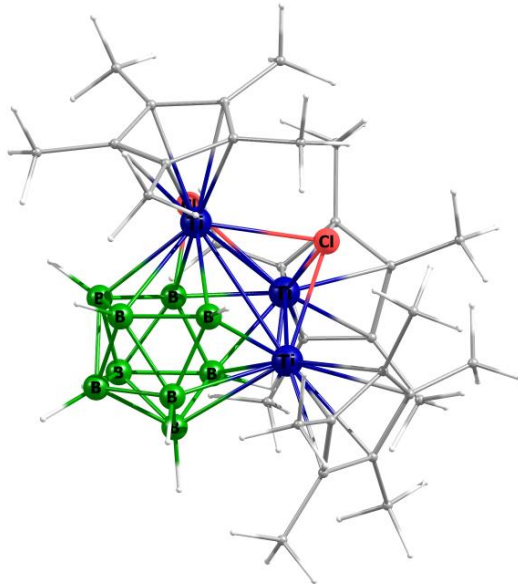


Figure S57. Optimized geometry of **1**.

Total energy = -4868.87421928 a.u.

Cartesian coordinates for the calculated structure **1** (in Å)

C	3.476540000	-0.442368000	1.661539000	H	-1.347465000	-4.578216000	1.067327000
C	4.220380000	-0.165276000	0.474475000	H	-2.813521000	-4.720324000	2.051302000
C	4.192282000	-1.340544000	-0.347271000	C	-2.663372000	-4.081119000	-1.495165000
C	3.455108000	-2.348853000	0.350838000	H	-3.540420000	-4.739975000	-1.614688000
C	2.995263000	-1.793415000	1.588347000	H	-1.836884000	-4.703685000	-1.127371000
C	3.335496000	0.473550000	2.840159000	H	-2.390428000	-3.719440000	-2.496718000
H	3.354864000	1.527511000	2.533119000	C	-4.363466000	-1.498631000	-2.237648000
H	4.165022000	0.321132000	3.552590000	H	-3.775777000	-1.911659000	-3.068154000
H	2.399708000	0.300226000	3.390240000	H	-4.476192000	-0.421944000	-2.421523000
C	5.066730000	1.042613000	0.218553000	H	-5.370267000	-1.950796000	-2.286178000
H	4.781808000	1.884180000	0.862221000	C	-4.929227000	0.092629000	0.435324000
H	4.986619000	1.377828000	-0.824583000	H	-5.949736000	-0.322788000	0.513749000
H	6.126363000	0.808084000	0.421339000	H	-4.919853000	0.759766000	-0.435562000
C	4.978697000	-1.544681000	-1.607966000	H	-4.761472000	0.699451000	1.334291000
H	6.010510000	-1.856792000	-1.367822000	C	-3.390429000	-1.378541000	2.842663000
H	5.032363000	-0.623298000	-2.201624000	H	-4.229375000	-1.901619000	3.333106000
H	4.537142000	-2.323163000	-2.244809000	H	-3.543297000	-0.302361000	2.992227000
C	3.311552000	-3.777648000	-0.090095000	H	-2.473880000	-1.663469000	3.379081000
H	3.157669000	-3.863926000	-1.175478000	C	-1.577653000	2.891837000	1.421959000
H	2.475388000	-4.284277000	0.411464000	C	-2.022707000	3.312723000	0.132280000
H	4.226930000	-4.344771000	0.152266000	C	-0.929841000	3.958860000	-0.527961000
C	2.292695000	-2.541319000	2.685598000	C	0.189650000	3.965187000	0.367424000
H	3.020913000	-3.040659000	3.348339000	C	-0.203776000	3.287860000	1.560402000
H	1.625944000	-3.322723000	2.292641000	C	-2.416847000	2.356036000	2.543395000
H	1.687470000	-1.872981000	3.314089000	H	-1.899904000	1.569283000	3.112278000
C	-2.737192000	-2.926980000	0.860893000	H	-3.366717000	1.942949000	2.180663000
C	-2.988545000	-2.955004000	-0.556088000	H	-2.663402000	3.160329000	3.258744000
C	-3.722126000	-1.775735000	-0.906881000	C	-3.422505000	3.278607000	-0.409060000
C	-3.938631000	-1.026058000	0.306449000	H	-3.826954000	4.303174000	-0.474806000
C	-3.326025000	-1.740504000	1.387688000	H	-4.095930000	2.702990000	0.235663000
C	-2.068110000	-4.003568000	1.665328000	H	-3.471810000	2.854944000	-1.423896000
H	-1.533335000	-3.593300000	2.533757000	C	-1.031824000	4.729462000	-1.810192000

H	-1.777639000	4.296879000	-2.490252000	B	-0.313624000	1.440177000	-2.782191000
H	-0.073959000	4.753883000	-2.344682000	H	-1.050840000	2.172869000	-3.392331000
H	-1.333277000	5.771648000	-1.601002000	B	-0.004316000	-0.248106000	-3.334323000
C	1.446246000	4.754472000	0.167118000	H	-0.476197000	-0.868184000	-4.245971000
H	2.225238000	4.471809000	0.886428000	B	1.283237000	0.942510000	-3.419397000
H	1.236820000	5.829666000	0.306513000	H	1.698715000	1.254574000	-4.499626000
H	1.856182000	4.615840000	-0.842480000	B	0.216103000	-0.897006000	-1.696430000
C	0.604252000	3.172119000	2.819579000	B	-1.081203000	0.109462000	-1.960081000
H	0.397262000	4.021595000	3.494200000	B	1.895528000	1.581509000	-0.603288000
H	1.681957000	3.175830000	2.610629000	H	2.606426000	2.317633000	0.036323000
H	0.373242000	2.252847000	3.376946000	Cl	0.225707000	-2.645325000	-0.750583000
B	1.614677000	-0.621653000	-2.610871000	Cl	-0.059471000	-0.168995000	1.471321000
H	2.207136000	-1.562933000	-3.076313000	Ti	1.897535000	-0.622775000	-0.176971000
B	2.448814000	0.834450000	-2.066121000	Ti	-1.608734000	-1.093595000	-0.213014000
H	3.596015000	1.010797000	-2.392870000	Ti	-0.292500000	1.630462000	-0.191800000
B	1.189100000	2.135865000	-2.091167000	H	-1.882397000	0.557464000	-1.204823000
H	1.431319000	3.271207000	-2.412046000				

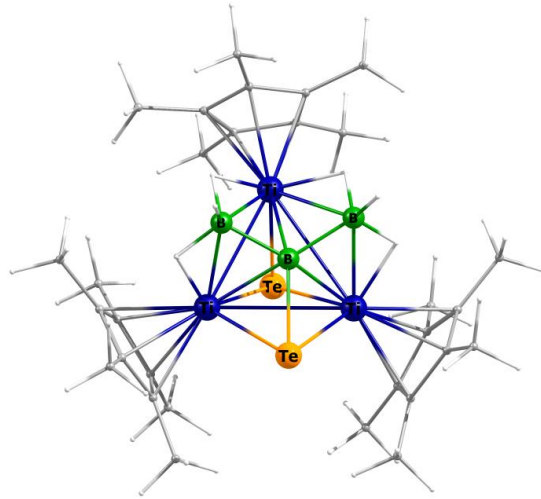


Figure S58. Optimized geometry of **2**

Total energy = -4332.65686166 a.u.

Cartesian coordinates for the calculated structure **2** (in Å)

C	-1.714365000	3.038749000	1.300385000	C	-3.225185000	3.736493000	-0.718030000
C	-0.317777000	3.172484000	1.641286000	H	-3.717053000	4.686125000	-0.408957000
C	0.351439000	3.786402000	0.520815000	H	-3.925929000	2.911210000	-0.482399000
C	-0.628485000	4.027018000	-0.505838000	H	-3.109740000	3.769160000	-1.819467000
C	-1.903961000	3.571970000	-0.016218000	C	-2.708094000	-2.894849000	0.516150000
C	-2.798612000	2.591584000	2.241364000	C	-2.861973000	-3.110646000	-0.902727000
H	-2.457990000	1.770559000	2.904077000	C	-3.661865000	-2.039901000	-1.430584000
H	-3.695448000	2.235176000	1.696735000	C	-4.034546000	-1.181554000	-0.328503000
H	-3.125464000	3.431973000	2.895359000	C	-3.459252000	-1.715534000	0.867550000
C	0.282468000	2.978327000	3.008377000	C	-2.058269000	-3.844052000	1.487448000
H	1.334360000	2.632583000	2.957749000	H	-2.791314000	-4.589858000	1.872152000
H	-0.278388000	2.233437000	3.606247000	H	-1.636332000	-3.311362000	2.363128000
H	0.277150000	3.936769000	3.576989000	H	-1.232661000	-4.416119000	1.017701000
C	1.771623000	4.287216000	0.533978000	C	-2.432854000	-4.340536000	-1.660370000
H	1.834604000	5.268734000	1.057245000	H	-1.517275000	-4.796641000	-1.233828000
H	2.170709000	4.434512000	-0.489091000	H	-2.227271000	-4.123230000	-2.727166000
H	2.454232000	3.591334000	1.062384000	H	-3.232407000	-5.114470000	-1.627789000
C	-0.386913000	4.722337000	-1.818447000	C	-4.145850000	-1.918726000	-2.851058000
H	-1.052509000	4.340316000	-2.618819000	H	-3.400441000	-2.302366000	-3.576596000
H	0.656227000	4.588081000	-2.168534000	H	-4.358763000	-0.866631000	-3.127341000
H	-0.569919000	5.817345000	-1.731402000	H	-5.084439000	-2.497742000	-3.005755000

C	-4.986647000	-0.020175000	-0.417081000	H	5.292855000	-2.486743000	-2.062566000
H	-4.847535000	0.690975000	0.421187000	C	2.722329000	-4.264986000	-0.401005000
H	-6.042875000	-0.370612000	-0.377782000	H	1.770128000	-4.652009000	0.014815000
H	-4.867331000	0.546773000	-1.362349000	H	3.528355000	-4.960446000	-0.075545000
C	-3.743846000	-1.255619000	2.270293000	H	2.655474000	-4.331343000	-1.504746000
H	-4.593565000	-1.834243000	2.698994000	C	2.138446000	-3.122801000	2.516621000
H	-4.020976000	-0.184510000	2.310669000	H	2.912931000	-3.711741000	3.058579000
H	-2.874058000	-1.398942000	2.942652000	H	1.371869000	-3.840157000	2.161609000
C	3.335082000	-1.037257000	1.470480000	H	1.650249000	-2.454889000	3.254003000
C	3.956878000	-0.738141000	0.206668000	Te	1.841049000	1.334267000	-1.695503000
C	3.744870000	-1.860669000	-0.671459000	Te	-0.244263000	-0.338782000	1.648536000
C	3.016482000	-2.862947000	0.064610000	B	0.276390000	-1.802374000	-1.982345000
C	2.757352000	-2.351181000	1.382903000	H	1.198035000	-2.374407000	-1.314187000
C	3.428264000	-0.190040000	2.710143000	H	-0.744818000	-2.455446000	-1.564660000
H	4.371409000	-0.401877000	3.263588000	H	0.428611000	-2.233122000	-3.120812000
H	2.584896000	-0.377615000	3.403922000	B	-1.413947000	0.691723000	-2.178401000
H	3.427308000	0.892598000	2.471026000	H	-1.504536000	1.875856000	-1.700862000
C	4.873499000	0.427539000	-0.053790000	H	-2.463796000	0.055317000	-1.843986000
H	4.532843000	1.352847000	0.452958000	H	-1.578699000	0.894792000	-3.378261000
H	4.964806000	0.652704000	-1.134647000	Ti	-0.424531000	1.670714000	-0.209778000
H	5.897029000	0.203027000	0.324278000	Ti	-1.624813000	-1.097290000	-0.656001000
C	4.286048000	-2.010629000	-2.067892000	Ti	1.609284000	-0.948791000	-0.210921000
H	4.385455000	-1.030199000	-2.575344000	B	0.076734000	-0.097829000	-1.699728000
H	3.626810000	-2.639490000	-2.699549000				

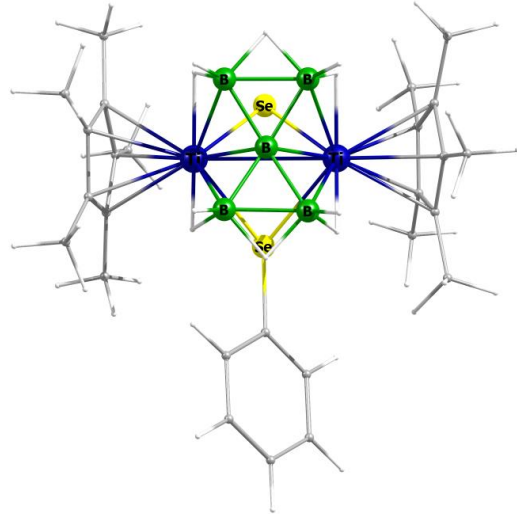


Figure S59. Optimized geometry of **3a**.

Total energy = -7643.59331474 a.u.

Cartesian coordinates for the calculated structure **3a** (in Å)

C	3.818880000	-1.229890000	0.782802000	C	-4.249092000	-0.656452000	2.516422000
C	3.797189000	0.192121000	0.588503000	H	-3.953469000	0.278414000	3.030772000
C	3.390606000	0.451452000	-0.767896000	H	-3.826246000	-1.498915000	3.098666000
C	3.183337000	-0.817203000	-1.418249000	H	-5.358060000	-0.733505000	2.577518000
C	3.439849000	-1.856326000	-0.461644000	C	-0.013396000	3.036965000	-0.262706000
C	4.328053000	-1.930054000	2.013653000	C	0.844781000	3.589576000	0.711263000
H	5.440041000	-1.981673000	1.996531000	H	1.569487000	2.951444000	1.235691000
H	3.950270000	-2.967713000	2.089767000	C	0.788929000	4.962120000	1.018325000
H	4.036698000	-1.405039000	2.944875000	H	1.467327000	5.372758000	1.783791000
C	-3.794245000	-0.678226000	1.081474000	C	-0.120450000	5.805044000	0.357721000
C	-3.603636000	-1.858430000	0.279320000	H	-0.162868000	6.878209000	0.602038000
C	-3.284534000	-1.444306000	-1.058282000	C	-0.968319000	5.266227000	-0.626372000
C	-3.307409000	-0.004555000	-1.092022000	H	-1.677310000	5.916823000	-1.163758000
C	-3.625212000	0.469943000	0.226344000	C	-0.910767000	3.896841000	-0.937532000

H	-1.558967000	3.490927000	-1.730878000	H	-3.080733000	1.898343000	-2.113718000
C	4.297672000	1.211504000	1.576072000	H	-4.121554000	0.713591000	-2.956968000
H	3.875117000	2.218153000	1.386929000	H	-2.339845000	0.516868000	-2.972849000
H	5.404773000	1.304561000	1.507169000	C	-3.890066000	1.901993000	0.607778000
H	4.054901000	0.936711000	2.621337000	H	-3.191263000	2.604375000	0.112032000
C	3.410807000	1.785619000	-1.461567000	H	-3.797617000	2.061065000	1.699744000
H	3.220697000	2.625553000	-0.765326000	H	-4.922997000	2.198001000	0.317194000
H	2.649037000	1.844303000	-2.264178000	B	-0.852373000	-2.253448000	2.277714000
H	4.405206000	1.962541000	-1.930626000	B	0.027058000	-0.803484000	2.045255000
C	2.895362000	-1.001190000	-2.881595000	B	0.929909000	-2.243592000	2.270210000
H	2.186521000	-0.237358000	-3.259779000	B	0.932641000	0.558002000	2.530131000
H	2.457174000	-1.995498000	-3.094288000	B	-0.855532000	0.579942000	2.529707000
H	3.833276000	-0.911101000	-3.475330000	Se	-0.003717000	-1.873824000	-1.145535000
C	3.454865000	-3.332437000	-0.753801000	Se	0.018827000	1.163156000	-0.886750000
H	4.428148000	-3.634589000	-1.201556000	Ti	-1.509085000	-0.661915000	0.401387000
H	2.655181000	-3.616961000	-1.466632000	Ti	1.539891000	-0.638598000	0.360242000
H	3.313507000	-3.937772000	0.163431000	H	-1.475552000	-2.453676000	1.195886000
C	-3.869770000	-3.274506000	0.714622000	H	1.549554000	-2.446710000	1.186566000
H	-3.715326000	-3.412116000	1.802314000	H	0.038687000	-3.250413000	2.102104000
H	-3.220432000	-4.001453000	0.187069000	H	1.579377000	-2.510448000	3.261313000
H	-4.924344000	-3.552373000	0.491619000	H	-1.499585000	0.680695000	3.555900000
C	-3.174932000	-2.339261000	-2.260751000	H	1.595209000	0.648786000	3.546326000
H	-4.171903000	-2.472165000	-2.739281000	H	1.589108000	0.931963000	1.510582000
H	-2.795486000	-3.345894000	-1.996119000	H	-1.499301000	0.970863000	1.508840000
H	-2.489119000	-1.921102000	-3.024010000	H	0.048365000	1.583629000	2.550295000
C	-3.199430000	0.822043000	-2.342550000	H	-1.500110000	-2.526851000	3.269782000

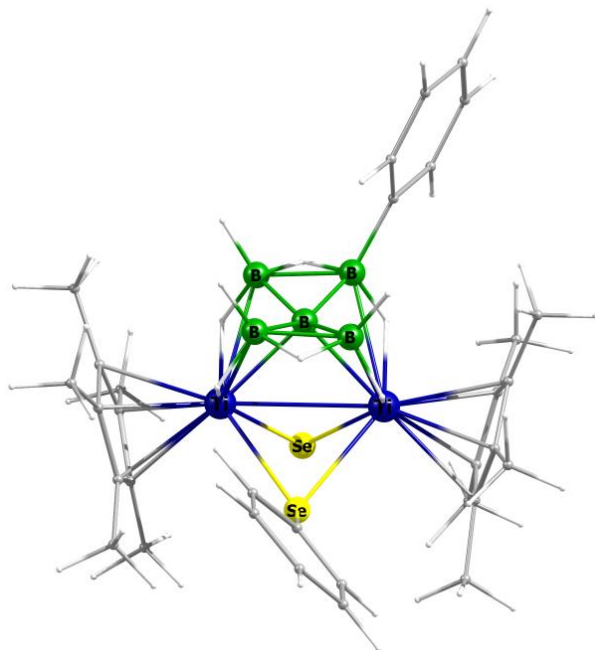


Figure S60. Optimized geometry of **3b**.

Total energy = -7874.48302201 a.u.

Cartesian coordinates for the calculated structure **3b** (in Å)

C	-3.797294000	-1.397733000	1.181910000	C	-5.149041000	-1.455812000	3.241600000
C	-4.977953000	-1.712616000	0.461187000	H	-5.206124000	-1.359508000	4.338259000
H	-4.926388000	-1.841231000	-0.633407000	C	-3.914966000	-1.285643000	2.588970000
C	-6.215842000	-1.888197000	1.104529000	H	-3.017577000	-1.060405000	3.185898000
H	-7.112947000	-2.136064000	0.513723000	C	2.056303000	-3.595868000	0.363230000
C	-6.306464000	-1.753665000	2.501230000	C	2.935820000	-2.641643000	0.975415000
H	-7.274288000	-1.888065000	3.010977000	C	3.480649000	-1.806218000	-0.063059000

C	2.948076000	-2.260527000	-1.321859000	C	1.384531000	-4.206918000	-2.103908000
C	2.062058000	-3.359377000	-1.061354000	H	2.078089000	-4.989016000	-2.486509000
C	1.401527000	-4.751906000	1.069543000	H	1.050896000	-3.601276000	-2.970170000
H	2.121357000	-5.594219000	1.178317000	H	0.493684000	-4.727417000	-1.699786000
H	0.523832000	-5.136927000	0.515734000	C	-4.143976000	0.848061000	-2.062706000
H	1.055228000	-4.480726000	2.086370000	H	-4.737387000	0.437966000	-1.223969000
C	-2.817929000	2.282824000	-0.307530000	H	-3.859692000	0.005715000	-2.725193000
C	-2.946977000	1.620872000	-1.580325000	H	-4.815991000	1.513933000	-2.649447000
C	-1.822018000	1.987643000	-2.393085000	C	-1.642876000	1.670573000	-3.850963000
C	-1.008957000	2.901605000	-1.634909000	H	-2.109521000	2.461788000	-4.481076000
C	-1.621379000	3.084932000	-0.347995000	H	-2.112440000	0.705752000	-4.126111000
C	-3.837519000	2.277190000	0.799954000	H	-0.572593000	1.606153000	-4.130784000
H	-3.372818000	2.441133000	1.791860000	C	0.153951000	3.670160000	-2.195848000
H	-4.392228000	1.320232000	0.853106000	H	0.704328000	4.215899000	-1.406027000
H	-4.584102000	3.088771000	0.646310000	H	-0.205746000	4.425658000	-2.930255000
C	2.466734000	2.167786000	1.135615000	H	0.878516000	3.013999000	-2.719160000
C	2.863537000	1.645076000	2.384673000	C	-1.184521000	4.068662000	0.704884000
H	2.704553000	0.582676000	2.615606000	H	-0.081640000	4.129498000	0.792694000
C	3.472755000	2.473049000	3.346232000	H	-1.581879000	3.804672000	1.704217000
H	3.773232000	2.044229000	4.316092000	H	-1.556545000	5.089227000	0.461598000
C	3.698650000	3.833343000	3.077081000	B	-2.392920000	-1.265947000	0.428120000
H	4.173602000	4.478751000	3.832762000	B	-0.841582000	-0.870791000	1.089065000
C	3.321591000	4.359513000	1.828714000	B	-1.124532000	-2.506762000	0.664161000
H	3.504733000	5.421241000	1.596521000	B	0.320548000	-0.794635000	2.340387000
C	2.717149000	3.533245000	0.865741000	B	-0.838629000	0.539309000	2.056063000
H	2.451628000	3.949557000	-0.119168000	Se	0.053236000	-0.713896000	-2.149124000
C	3.352510000	-2.646398000	2.421582000	Se	1.702352000	1.121469000	-0.356787000
H	3.729093000	-1.657600000	2.750480000	Ti	-0.987509000	0.764127000	-0.461618000
H	4.174024000	-3.379472000	2.585067000	Ti	1.082953000	-1.437033000	-0.004486000
H	2.520307000	-2.928693000	3.095952000	H	-2.422469000	-0.621898000	-0.668619000
C	4.590539000	-0.803746000	0.093624000	H	-0.302819000	-2.792649000	-0.255239000
H	4.605137000	-0.343809000	1.100775000	H	-2.169062000	-2.470370000	-0.175912000
H	4.510292000	0.019477000	-0.643950000	H	-1.304289000	-3.413837000	1.451538000
H	5.578187000	-1.294626000	-0.060286000	H	-1.684784000	0.856938000	2.868678000
C	3.369175000	-1.751072000	-2.671396000	H	0.326116000	-1.469364000	3.352929000
H	3.506275000	-0.650894000	-2.669537000	H	1.461039000	-0.781861000	1.786444000
H	2.624577000	-1.992196000	-3.454460000	H	-0.537354000	1.506576000	1.290041000
H	4.338373000	-2.209000000	-2.973369000	H	0.322372000	0.498671000	2.742099000

References

- 1 G. H. Llinás, M. Mena, F. Palacios, P. Royo and R. Serrano, *J. Organomet. Chem.*, 1988, **340**, 37.
2 R. Ramalakshmi, K. Saha, D. K. Roy, B. Varghese, A. K. Phukan and S. Ghosh, *Chem. Eur. J.*, 2015, **21**, 17191.
3 M. T. Mock, R. G. Potter, D. M. Camaioni, J. Li, W. G. Dougherty, W. S. Kassel, B. Twamley and D. L. DuBois, *J. Am. Chem. Soc.*, 2009, **131**, 14454.
4 (a) J. J. Led and H. Gesmar, *Chem. Rev.*, 1991, **91**, 1413; (b) L. Yang, R. Simionescu, A. Lough and H. Yan, *Dyes Pigm.*, 2011, **91**, 264; (c) R. Weiss and R. N. Grimes, *J. Am. Chem. Soc.*, 1978, **100**, 1401.
5 S. Kar, S. Bairagi, J.-F. Halet and S. Ghosh, *Chem. Commun.*, 2023, **59**, 11676.
6 P. Govindaswamy, Y. A. Mozharivskyj, M. R. Kollipara, *Polyhedron* **2005**, *24*, 1710.
7 P. Govindaswamy, Y. A. Mozharivskyj, M. R. Kollipara, *Polyhedron* **2005**, *24*, 1710.
8 a) C. E. Rao, S. K. Barik, K. Yuvaraj, K. Bakthavachalam, T. Roisnel, V. Dorcet, J.-F. Halet, Ghosh, *Eur. J. Inorg. Chem.* **2016**, 4913; b) A. Haridas, S. Kar, B. Raghavendra, T. Roisnel, V. Dorcet, S. Ghosh, *Organometallics* **2020**, *39*, 58.
9 S. Bairagi, S. Giri, G. Joshi, E. D. Jemmis and S. Ghosh, *Angew. Chem. Int. Ed.*, 2024, e202417170.
10 A. Altomare, G. Cascarano, C. Giacovazzo, A. Guagliardi, M. C. Burla, G. Polidori and M. Camalli, *J. Appl. Crystallogr.*, 1994, **27**, 435.
11 G. M. Sheldrick, *Acta Cryst.*, 2015, **C71**, 3.
12 O. V. Dolomanov, L. J. Bourhis, R. J. Gildea, J. A. K. Howard and H. Puschmann, *J. Appl. Cryst.*, 2009, **42**, 339.
13 M. J. Frisch, G. W. Trucks, H. B. Schlegel, G. E. Scuseria, M. A. Robb, J. R. Cheeseman, G. Scalmani, V. Barone, B. Mennucci, G. A. Petersson, H. Nakatsuji, M. Caricato, X. Li, H. P. Hratchian, A. F. Izmaylov, J. Bloino, G. Zheng, J. L. Sonnenberg, M. Hada, M. Ehara, K. Toyota, R. Fukuda, J. Hasegawa, M. Ishida, T. Nakajima, Y. Honda, O. Kitao, H. Nakai, T. Vreven, J. A. Montgomery Jr., J. E. Peralta, F. Ogliaro, M. Bearpark, J. J. Heyd, E. Brothers, K. N. Kudin, V. N. Staroverov, R. Kobayashi, J. Normand, K. Raghavachari, A. Rendell, J. C. Burant, S. S. Iyengar, J. Tomasi, M. Cossi, N. Rega, J. M. Millam, M. Klene, J. E. Knox, J. B. Cross, V. Bakken, C. Adamo, J. Jaramillo, R. Gomperts, R. E. Stratmann, O. Yazyev, A. J. Austin, R. Cammi, C. Pomelli, J. W. Ochterski, R. L. Martin, K. Morokuma, V. G. Zakrzewski, G. A. Voth, P. Salvador, J. J. Dannenberg, S. Dapprich, A. D. Daniels, Ö. Farkas, J. B. Foresman, J. V. Ortiz, J. Cioslowski, D. J. Fox, *Gaussian 09, Revision C.01*, Gaussian, Inc., Wallingford, CT, 2010.
14 (a) H. L. Schmid, A. D. Becke, *J. Chem. Phys.* 1998, **108**, 9624; (b) J. P. Perdew, *Phys. Rev. B: Condens. Matter Mater. Phys.* 1986, **33**, 8822.
15 EMSL Basis Set Exchange Library. <https://bse.pnl.gov/bse/portal>
16 F. London, *J. Phys. Radium.*, 1937, **8**, 397.
17 R. Ditchfield, *Mol. Phys.*, 1974, **27**, 789.
18 K. Wolinski, J. F. Hinton and P. Pulay, *J. Am. Chem. Soc.*, 1990, **112**, 8251.
19 (a) A. D. Becke, *Phys. Rev. A.*, 1988, **38**, 3098; (b) C. Lee, W. Yang and R. G. Parr, *Phys. Rev. B.*, 1988, **37**, 785; (c) A. D. Becke, *J. Chem. Phys.*, 1993, **98**, 5648.
20 T. P. Onak, H. L. Landesman, R. E. Williams and I. Shapiro, *J. Phys. Chem.*, 1959, **63**, 1533.
21 (a) E. D. Glendening, A. E. Reed, J. E. Carpenter and F. Weinhold, *NBO Program 3.1*, W. T. Madison, 1988; (b) A. E. Reed, F. Weinhold and L. A. Curtiss, *Chem. Rev.*, 1988, **88**, 899; (c) F. Weinhold and R. Landis, *Valency and bonding: A natural bond orbital donor-acceptor perspective*; Cambridge University Press: Cambridge, U.K, 2005.
22 K. Wiberg, *Tetrahedron*, 1968, **24**, 1083.
23 (a) R. F. W. Bader, *Atoms in Molecules: A Quantum Theory*; Oxford University Press: Oxford, U. K., 1990; (b) R. F. W. Bader, *J. Phys. Chem. A.*, 1998, **102**, 7314; (c) R. F. W. Bader, *Chem. Rev.*, 1991, **91**, 893.
24 T. Lu, F. Chen, *J. Comput. Chem.*, 2012, **33**, 580.
25 I. I. Dennington, R. T. Keith, J. Millam, K. Eppinnnett, W. L. Hovell and R. Gilliland, *GaussView, Version 3.09*; Semichem Inc.: Shawnee Mission, KS, 2003.
26 G. A. Zhurko, <http://www.chemcraftprog.com>.